MODELING MASS BALANCE AT ROBERTSON GLACIER,

ALBERTA, CANADA 1912-2012

by

Ryan Scott Scanlon

A thesis submitted in partial fulfillment
of the requirements for the degree

of

Master of Science

in

Earth Sciences

MONTANA STATE UNIVERSITY
Bozeman, Montana

April 2017

ACKNOWLEDGEMENTS

I would like to thank the following for helping me make this thesis possible. I would first like to thank my committee members, Dr. Mark Skidmore, Dr. Jordy Hendrikx, and Dr. Lucy Marshall for their insight, support, and encouragement throughout this process. I would also like to thank the Alpine Club of Canada, Montana State University College of Letters and Science, and the Montana State University Graduate School for providing a research grants that allowed this research to be completed and presented at several professional conferences. In addition, I would also like to thank Terra Spotts and Andrew Blessing for helping to gather field data. I would also like to thank Alberta Provincial Parks for allowing research to be conducted within Peter Lougheed Provincial Park. I would also like to thank Dr. John Borkowski for valuable insights into the statistical analysis performed in this study. Finally, I would like to thank my wife, Yujian Wang, for all of her support throughout this process.

ABSTRACT

Glacier mass balance is important to study due to the role of glaciers in the hydrological cycle. Glacier mass balance is typically difficult to measure without numerous *in situ* measurements and monitoring over the course of many years. Physically based melt models are a good tool for estimating melt using temperature, solar radiation, and albedo and are used extensively in this thesis. A Degree Day (DD) model and an Enhanced Temperature Index (ETI) model are used to model mass balance for Robertson Glacier, Alberta, Canada during the period 1912-2012. The DD model only incorporates temperature, while the ETI model incorporates temperature, incoming solar radiation, and albedo. Incoming solar radiation was modeled for the period 2007-2012 and parameterized for the period 1912-2006 while temperature was measured at the regional scale and synthesized for Robertson Glacier and the snowpack thickness was modeled using PRISM. The DD and ETI models both assume a static ice mass, i.e. no flow or change in ice elevation due to mass loss over the century time period. Both models estimate a high value of annual and accumulated mean mass loss for the period 1912-2012. Sensitivity analyses of model inputs indicate that snowpack is an important factor, and it appears PRISM estimates may underrepresent beginning of the year snowpack by 220% based on a comparison of modelled to measured values on the adjacent Haig Glacier. Avalanching is not a key component of accumulation on the Haig Glacier but is a key process at Robertson Glacier, and could result in locally doubling the snowpack accumulation in avalanche zones. These factors including the resultant albedo changes with a thicker snowpack are all part of a compounding negative feedback cycle on glacier mass loss. In summary, the thesis has highlighted several potential limitations to the ETI and DD models for assessing mass loss for a small mountain glacier in the southern Canadian Rockies and provides suggestions for future modelling work in this region.

TABLE OF CONTENTS

TABLE OF CONTENTS – CONTINUED

LIST OF TABLES

LIST OF TABLES – CONTINUED

LIST OF FIGURES

LIST OF FIGURES – CONTINUED

LIST OF FIGURES – CONTINUED

Figure Page

CHAPTER 1 – INTRODUCTION

Study Rationale

There are many reasons to study the cryosphere, primarily for its important role in the hydrological cycle at local, regional and global scales. Glaciers and ice caps account for 75% of the freshwater on Earth and cover approximately 10-11% of the Earth's surface (Cuffey & Paterson, 2010). Gardner et al. (2013) estimate that global glacier area, outside of the major ice sheets and ice caps is 729,400 km^2 and these glaciers are losing on average 350 kg m^{-2} $year^{-1}$ with glaciers of Western Canada and the United States losing on average 910 kg m^{-2} $year^{-1}$ during the period 2003-2009. Focusing on the Southern Canadian Rockies, the study region for the thesis, Bolch et al. (2010) estimated that glaciers of this region lost 235 km^2 of ice extent over the period 1985-2005. This equates to a loss of 14.8% during this period, while Alberta lost 25.4% of its glacial cover over the same time frame, 267 km^2 of ice extent. At the individual glacier level, there are few detailed mass balance records in the Southern Canadian Rockies. Peyto Glacier in Banff National Park, Alberta, Canada has the longest continual mass balance record in Canadian Rockies, and it has lost 29.2 m w.e. (water equivalent) of glacier thickness during the period 1966-1995 (Demuth et al. 2006). The mean thickness of Peyto Glacier was 95 m in 1999 (Demuth & Pietroniro, 1999). Collectively these datasets indicate significant mass loss for glaciers in the Southern Canadian Rockies over the past ~ 50 years.

Mass Balance and Hydrology

Glaciers act as natural reservoirs for snow, ice, and meltwater, which on an annual time scale can lead to increased late summer discharge in glacier-fed streams and rivers, which are likely enhanced during periods of strong negative mass balance. This glacial contribution to stream discharge plays an important role in the regional hydrological cycle (Ohmura, 2001), providing much of the base flow in late summer and early fall, after the seasonal snowpack has melted (Fountain & Tangborn 1985). Glaciers in the Himalaya are important for generating hydroelectricity and irrigation, for over 1 billion people (Srivastava et al. 2014), and fresh drinking water for 70 million people (United Nations, 2012). Ericksson, (2009) reported that glacier melt in the Himalaya region represent 2-50% of the river flow in the ten largest rivers in Asia.

Glacial contributions to streamflow are also important in the Southern Canadian Rockies. The Bow River basin in Alberta comprises a total area of 26,200 km^2 (Bow River, 2016), of which approximately 7,000 km^2 is upstream of Calgary, and Marshall et al. (2011) estimated water from melting glaciers accounted for 2.8% of annual flow in the Bow River, measured in Calgary. Note, these figures are based solely on glacier melt and they do not consider of seasonal glacier snowpack. This figure rises to 6.7% of the flow on average in July, August, and September, peak melt months. However, the Bow River basin is estimated to only be 0.76% glaciated upstream of Calgary (Marshall et al. 2011). Glacial melt contributions can change significantly in the upper reaches of a glacial-fed river, for example, the Bow River is comprised of more than 50% glacier fed water in

August at Banff, where the contributing basin size is 2,230 km^2 (Hopkinson &Young, 1998).

Mass Balance

Glacier volume and mass balance are commonly measured attributes in glaciological studies. Glacier mass balance is defined as the balance between accumulation, the deposition of solid precipitation contributing to the winter balance, and ablation, the melting of snow and ice which represents the summer balance in a given glaciological year, the start of the accumulation season to the end of the subsequent melt season, October 1 - September 30 in the northern hemisphere (Benn & Evans 2010). This balance varies spatially and temporally based primarily upon local temperature and precipitation, elevation, and latitude. In order to understand water loss via ablation, we must first know the initial ice volume. There are numerous ways to calculate glacier mass balance, such as the glaciological method, the process-model method, altimetric method, hydrological method, geological method, flux-gate method, and the gravitational method (Cuffey & Paterson, 2010). The three most commonly used are the glaciological, process-model, and the altimetric method. For this study a combination of the glaciological and process-model methods were used.

The glaciological method utilizes field measurements of annual snow accumulation and surface ablation via a network of points along the glacier surface. From this information surface mass balance, can be calculated via equation (1):

$$\dot{b}_S = \dot{a}_S - \dot{m}_S \tag{1}$$

where $\dot{b}_s$= surface balance in mm water equivalent (w.e.) year^{-1}, $\dot{a}_s$= snowpack in mm w.e. year^{-1}, and $\dot{m}_S$ =melt in mm w.e. year^{-1}. This equation gives a good approximation of surface balance (Cuffey & Patterson, 2010). This method has been used extensively to study mass balance of glaciers around the world (e.g. Tangborn et al, 1971; Young 1981; Fountain & Vecchia 1999).

Glaciers and ice sheets are typically located in areas that are relatively inaccessible and thus scientists are driven to find the most efficient ways to study them without the need for *in situ* measurements and this is where process-models are useful. There are three different process-models: degree day (DD), enhanced temperature index (ETI), and full energy balance model. The DD model is the most widely used both historically and spatially, examples include; Ostrem (1964) at Nigardsbreen, Norway, Braithwaite & Olesen (1989) in West Greenland, and Hock (1999) at Storglaciären, Sweden. A typical DD model (Cuffey and Paterson, 2010) takes the form of:

$$M = \begin{cases} (DDF) * T & T > 0°C \\ 0 & T \leq 0°C \end{cases} \tag{2}$$

where M= melt in mm w.e. day^{-1}, DDF = degree day factor in mm w.e. °C^{-1} day^{-1}, and T = average daily air temperature. It is assumed that no melt occurs when the temperature is below 0°C.

The DD model is widely used, primarily due to its simplicity as minimal input, i.e. temperature, is required to estimate melt. Hock (2003) cites four reasons why a temperature index model such as the DD model is prevalent: (1) wide availability of air temperature data, (2) relatively easy interpolation and forecasting possibilities of air temperature, (3) generally good model performance despite their simplicity and (4) computational simplicity. Braithwaite & Olesen (1989) in a study in west Greenland found a correlation coefficient of 0.96 between annual ice ablation and positive average daily air temperatures. This method provides melt estimates for remote areas much more easily than using the glaciological method which requires physical measurements of snow density and surface lowering. The DD model relies on the assumed linear relationship between positive air temperature and ablation rate, which has some drawbacks. First, temporal resolution is restricted to longer time periods; Lang (1986) noted that accuracy decreases with increasing temporal resolution, single days are not modeled accurately, thus a week time scale or longer is needed. The second major drawback is that spatial variability; topographic shading, aspect, slope angle, in melt rates is not modelled accurately (Hock, 1999).

A newer approach to melt modelling, the ETI, incorporates solar radiation in addition to temperature (Hock, 1999). The ETI tries to eliminate some of the limitations in terms of spatial variability that Hock (1999) noted for the DD model. The ETI used in this study is from Pellicciotti et al. (2005) and takes the form:

$$M = \begin{cases} (TF) * T + [SRF * (1 - \alpha) * G] & T > 1°\text{C} \\ 0 & T \leq 1°\text{C} \end{cases} \qquad (3)$$

where M is the melt rate in mm h^{-1}, TF is the temperature factor and is expressed in mm h^{-1} $°C^{-1}$, SRF is the shortwave radiation factor and is expressed in m^2 mm W^{-1} h^{-1}, α is albedo, and G is incoming shortwave radiation in Wm^{-2}. In the ETI model outlined in Pellicciotti et al. (2005) air temperatures of 1°C.or higher are required for melt to occur.

The full energy balance model is the most robust model for calculating surface melt (Hock & Holmgren, 2005). Temperature does not solely define melt; wind speed, humidity, cloud, snowfalls, and albedo all play a role (Cuffey & Paterson, 2010). The full energy balance model takes the form:

$$E_N = E_S^{in} + E_S^{out} + E_L^{in} + E_L^{out} + E_G + E_H + E_E + E_P \tag{4}$$

where E_N is net energy flux, E_S^{in} and E_L^{in} are incoming shortwave and longwave radiation, respectively, while E_S^{out} and E_L^{out} are outgoing shortwave and longwave radiation respectively. The sum of all radiation terms ($E_S^{in} + E_S^{out} + E_L^{in} + E_L^{out}$) gives the net radiation E_R. $E_G, E_H, E_E, and\ E_P$ are subsurface energy flux, sensible heat flux, latent heat flux, and heat flux from precipitation, respectively. These terms are not specifically parameterized in either the DD model and the ETI model. Ohmura (2001) found that E_G represents about 10% of melt energy on cold glaciers - a cold glacier is one that is frozen to its bed (Benn and Evans 2010), - such as the Hans Tausen Icecap and Kronprins Christian Land, Greenland. The terms E_H and E_E represent the turbulent heat fluxes, which can contribute 40% and 60% of the melt energy on Alpine glaciers, as shown for 1993 and 1994 at Storglaciären, Sweden (Hock & Holmgren, 2005). The main drawback of the full energy balance model is the advanced and complex field instrumentation required to generate the necessary input data. This instrumentation, effectively a number of well-equipped meteorological stations, is costly and difficult to place on a glacier with sufficient density to accurately represent conditions for the entire glacier.

<u>Study Location</u>

Robertson Glacier, Alberta, Canada was chosen for this study because it is characteristic of glaciers in the Southern Canadian Rockies. It has a simple geometry, modest size and is relatively accessible, thus making the study feasible for travel and cost. Robertson Glacier is also adjacent to an Automatic Weather Station (AWS) that has been in operation since 2007, thus providing historical data in addition to the field data collected in this study. Finally, Robertson Glacier was chosen as there was an associated research project on glacial chemistry and microbiology occurring concurrently, which was beneficial for logistics.

The goal of the thesis is to determine the most robust model to provide accurate estimates of mass balance for Robertson Glacier in the Canadian Rockies with the fewest number of measured inputs required. The goal of this study is to compare the DD model and ETI model for Robertson Glacier using differing combinations of measured data, modelled data and parameterized data. The DD model, relying only on air temperature, uses measured data for part of the 2012 melt season, July 8th - September 25th, and modeled temperature for the remainder of the 2012 melt season and the period from 1912-2011. This time period was chosen because it was the longest record of reliable data that was available from the Banff automatic weather station (AWS). The ETI uses measured temperature values for the same period of the 2012 melt season, July 8th – September 25th, and modeled temperature for the remainder of 2012 and the period from 1912-2011. Incoming solar radiation was modeled based upon measurements taken down valley at an AWS for the period of 2006-2012, an average of the daily modelled values was then taken to generate daily estimates for the period 1912-2005. Albedo was parameterized based upon *in situ* observations of the surface cover at the glacier during July 8th – September 25th, 2012.

This study also used surface area-volume relationships from Bahr et al. (1997) and Marshall et al. (2011) to determine estimated glacier thickness and melt estimates from ETI and DD models to forecast potential ice cover duration for a given elevation on Robertson Glacier, assuming the ice mass remains static.

CHAPTER 2 – METHODS

Study Site

The Canadian Rockies are a heavily glaciated mountain range running from North to South with the continental divide (Ommanney, 2001). The range has 37 peaks reaching above 3400 meters above sea level, and runs along the border between British Columbia and Alberta (Ommanney, 2001). The study site for this thesis was Robertson Glacier, Alberta, (50°43’50” N, 115°19’52” W) (Figure 2.1) immediately on the lee side of the continental divide. Robertson Glacier is approximately 1930 m long and 860 m at the widest point with an elevation range of approximately 500 m from 2366 m at the terminus to 2900 meters at the continental divide. The average slope along the length of the glacier is 15° with an aspect of 340°. Robertson Glacier is flanked by high ridge lines on the east and west that provide significant shading throughout the day, these ridgelines provide a vertical relief of 500m at the terminus of the glacier and 300m at the col. A hypsometric profile of Robertson Glacier can be seen in Figure 2.2. This was created by calculating the cumulative ice area as a function of elevation in ArcGIS.

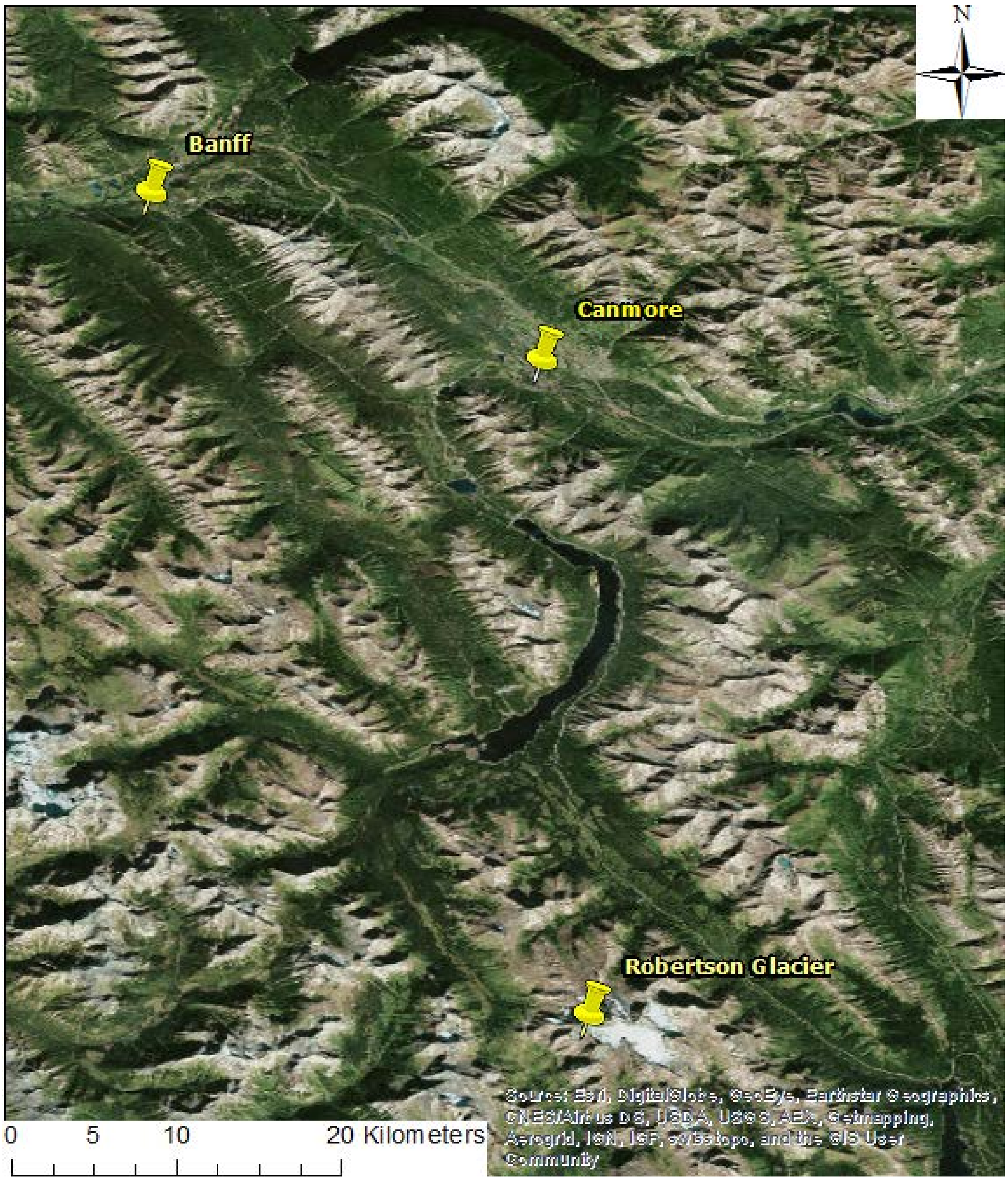

Figure 2.1. Location of Robertson Glacier relative to Canmore and Banff, Alberta, Canada (Google, 2016).

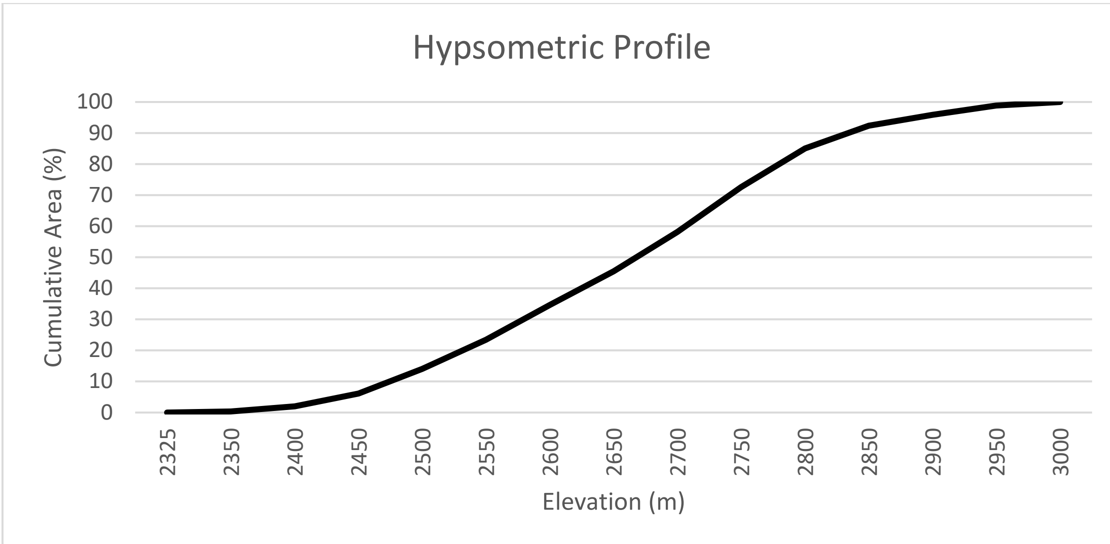

Figure 2.2. Hypsometric profile of Robertson Glacier measured along the centerline of the glacier.

Robertson Glacier is in Peter Lougheed Provincial Park, and this region of the Canadian Rockies is blocked from maritime climatic influences by the Coast Range although it is only 700 km from the Pacific Ocean. The Southern Canadian Rockies are characterized by a continental climatic regime with precipitation amounts ranging from 285 mm snow water equivalent (SWE) to 864 mm SWE and a large range in average daily temperature, from -30°C to 22°C over the year (Young, 1981). The weather conditions at Robertson Glacier are dominated by mid-latitude cyclones crossing the region from west to east (Yarnal, 1984) and orographic uplift on the western slopes of the Rockies inducing precipitation (Marshall et al., 2011). Robertson Glacier is on the lee of the continental divide but likely receives similar precipitation to the Haig Glacier, adjacent to Robertson Glacier, but on the windward side of the continental divide, given the col separating the ice masses has a low relief ~ 50m. Haig Glacier receives upwards of 1800 mm SWE annually near the Continental Divide at an elevation of 2800 m (Shea et al. 2005), while the highest SWE measured at Three Isle Lake, the closest Environment Canada snow pillow site 12 km south of Robertson Glacier at an elevation of 2160 m, is 675 mm SWE. The Three Isle Lake snow survey location is on the lee side of the Continental Divide.

Field Methods

Snow and Ice Melt Data Collection

Surface melt was measured during the period from July 8th – September 25th 2012 via a network of ablation stakes. Fourteen white PVC stakes were drilled into the ice along three transects of the glacier. One transect followed the longitudinal profile of the glacier roughly along the centerline with stakes placed at roughly 50 meter vertical intervals, with the other two transects being approximately parallel to flow at elevations of 2400 meters and 2500 meters. Three stakes at elevations of 2504, 2642 and 2866 m had complete data sets for the period July 8th – September 25th 2012 and were used in this analysis (Figure 2.3; Table 2.1). Measurements of ice surface lowering were taken via the straight-edge method (Kaser et al. 2003) at weekly or bi-weekly intervals. Snow density measurements were made twice during the melt season with a Wasatch snow density gauge, once when stakes were drilled, July 8th, 2012 and again mid-way through the melt season, August 8th, 2012. Three measurements of snow density were made; one at the terminus of the glacier, 2366 m, one adjacent to the stake at 2504 m, and one adjacent to the stake at 2642 m. The Wasatch snow density gauge was used because of it's compact size, and portability. The components consist of a 100 cm^3 cylindrical cutter and mass balance scale reading from 0% to 60% water content.

Table 2.1. Elevation of ablation stakes and automatic weather stations (AWS) and duration of data record.

Station	Elevation (m)	Location	Period of Functioning
Banff AWS	1396	50 km from glacier	01 January 1912-present
Robertson AWS	2062	Outwash Plain	01 August 2005-present
8	2504	Glacier	08 July-25 September 2012
11	2642	Glacier	08 July-25 September 2012
15	2866	Glacier	08 July-25 September 2012

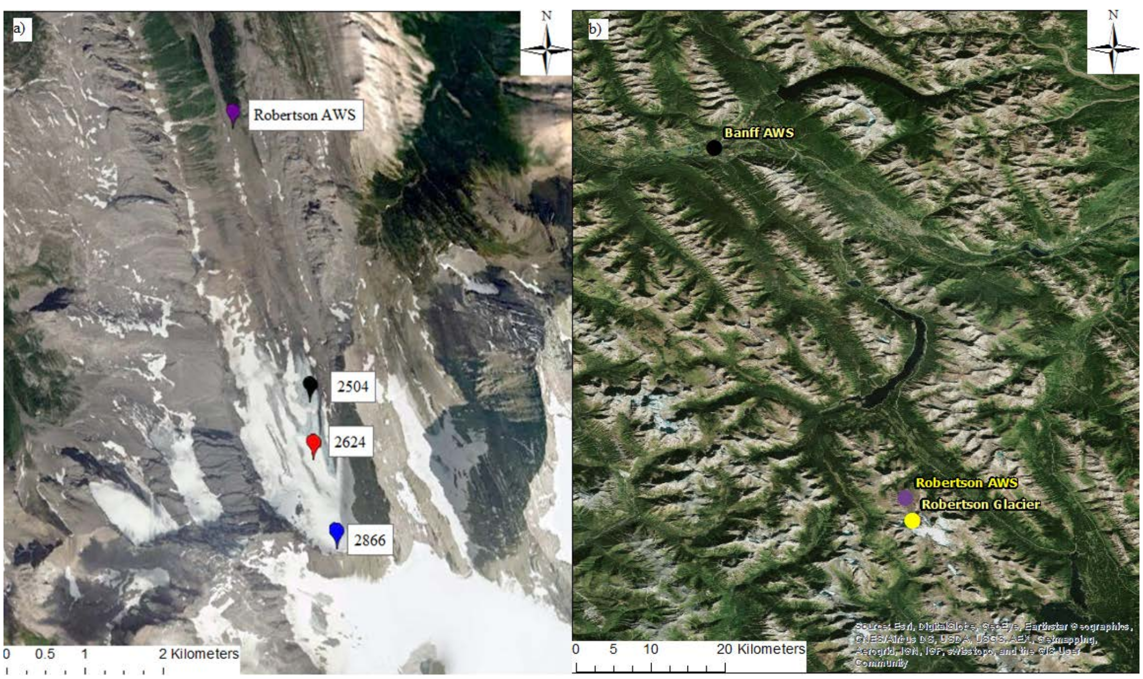

Figure 2.3 a. Location of the three ablation stakes with temperature and relative humidity sensors and data loggers, and the Robertson AWS (Google, 2016). b. Location of Banff AWS relative to location of glacier data loggers and Robertson AWS (Google, 2016).

Automatic Weather Station and Data Loggers

HOBO U23 Pro™ External Temperature/Relative Humidity Data Loggers, Figure 2.4a, placed into white solar radiation shields were deployed on each of the 14 ablation stakes. These data loggers recorded temperature and relative humidity at 15 minute intervals from July 8th-September 25th 2012, and the data was used to generate daily averages of these parameters. The loggers were kept at between 0.5-2.0 meters above the ice or snow surface in order to accurately measure surface temperature as outlined in Marshall et al., (2007). The manufacturer's stated accuracy for the loggers is ±0.2°C for temperature measurements and ±2.5% for relative humidity (Onset, 2010).

An automatic weather station (AWS) from Queens University approximately one km down valley from the glacier terminus has been operational since August, 2005 (Figure 2.4b, Table 2.1). The automatic weather station is equipped to record the following meteorological values: air temperature (°C), relative humidity (%), wind speed (m s^{-1}) and direction (°), incoming solar radiation (kJ m^{-2}), barometric pressure (mbar), and rainfall (mm). Measurements are taken every 15 minutes and the averages stored hourly and daily on a Campbell CR100 data logger. The sensors were mounted on a tripod and an arm 1.5-2.0 meters above the ground (Figure 2.4b).

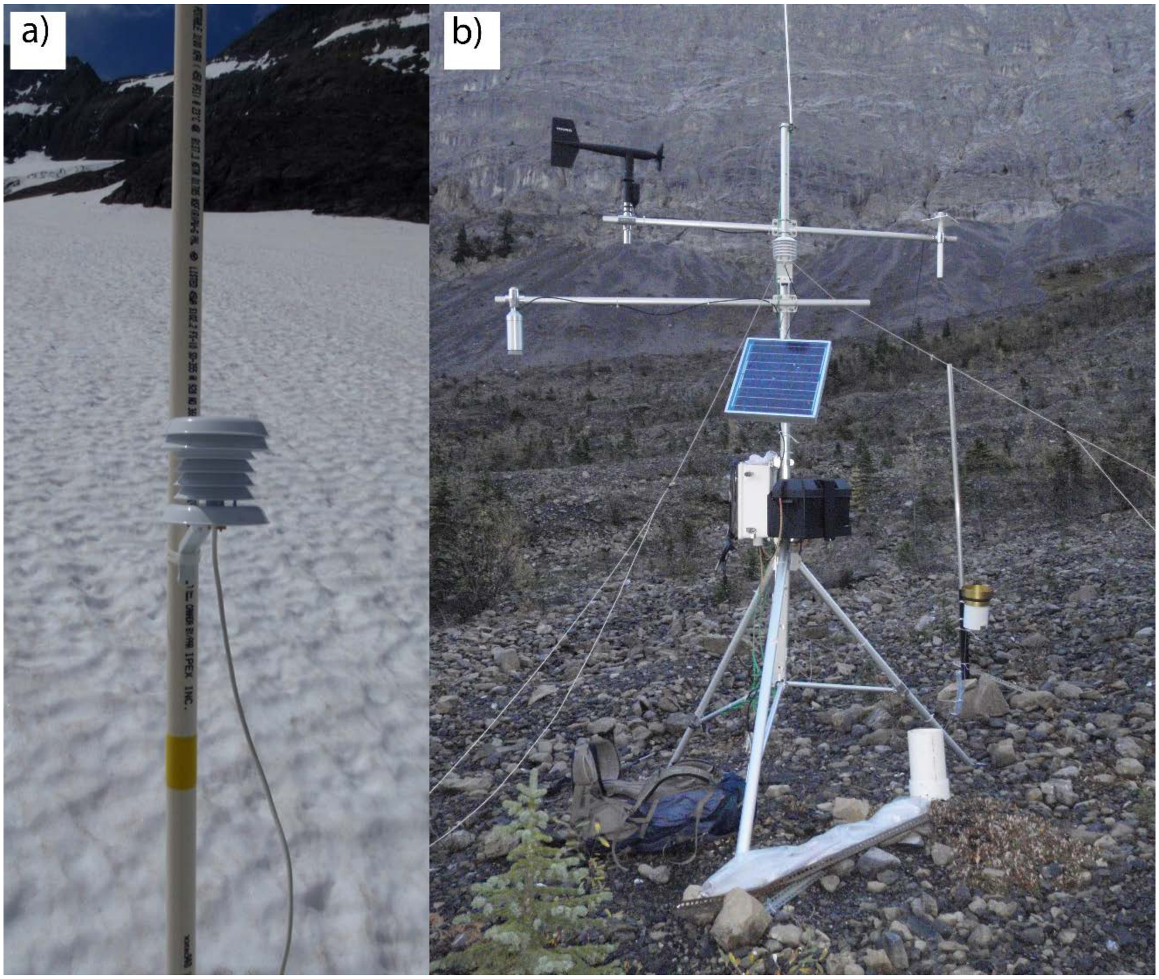

Figure 2.4 a. HOBO U23 Pro deployed on an ablation stake on Robertson Glacier. 2.4b. Robertson AWS 1 km down valley from Robertson Glacier (Elevation 2062m).

Time Lapse Camera

Two Canon Rebel T3 cameras (Table 2.2) equipped with a Harbortronics DigiSnap 2700 intervalometer were placed inside a fiberglass housing and set to take a photo every daylight hour. The two cameras at elevations of 2361 m and 2527 m were deployed on 3 July 2012 and taken down on 26 September 2012 (Figure 2.5). The cameras were set to take photos with the widest field of view possible, 18 mm focal length, thus showing the effects of shading throughout the day and surface cover, snow or ice during the melt season.

Table 2.2. Specifications of Time Lapse Camera.

Model	**Canon EOS T3 Rebel**
Sensor Type	Large single-plate CMOS sensor
CCD effective pixels	12.20 megapixels
CCD Color Filter Array	RGB Primary color filters
Image ratio w:h	3:2
File format	JPEG
Zoom	18-55 mm
Lens Aperture	f/3.5-5.6
Focus Range	0.25 m to infinity
Autofocus type	9 Points
ISO Speed Range	Auto, ISO 100-6400
Exposure Compensation	±5 stops
Storage	SD

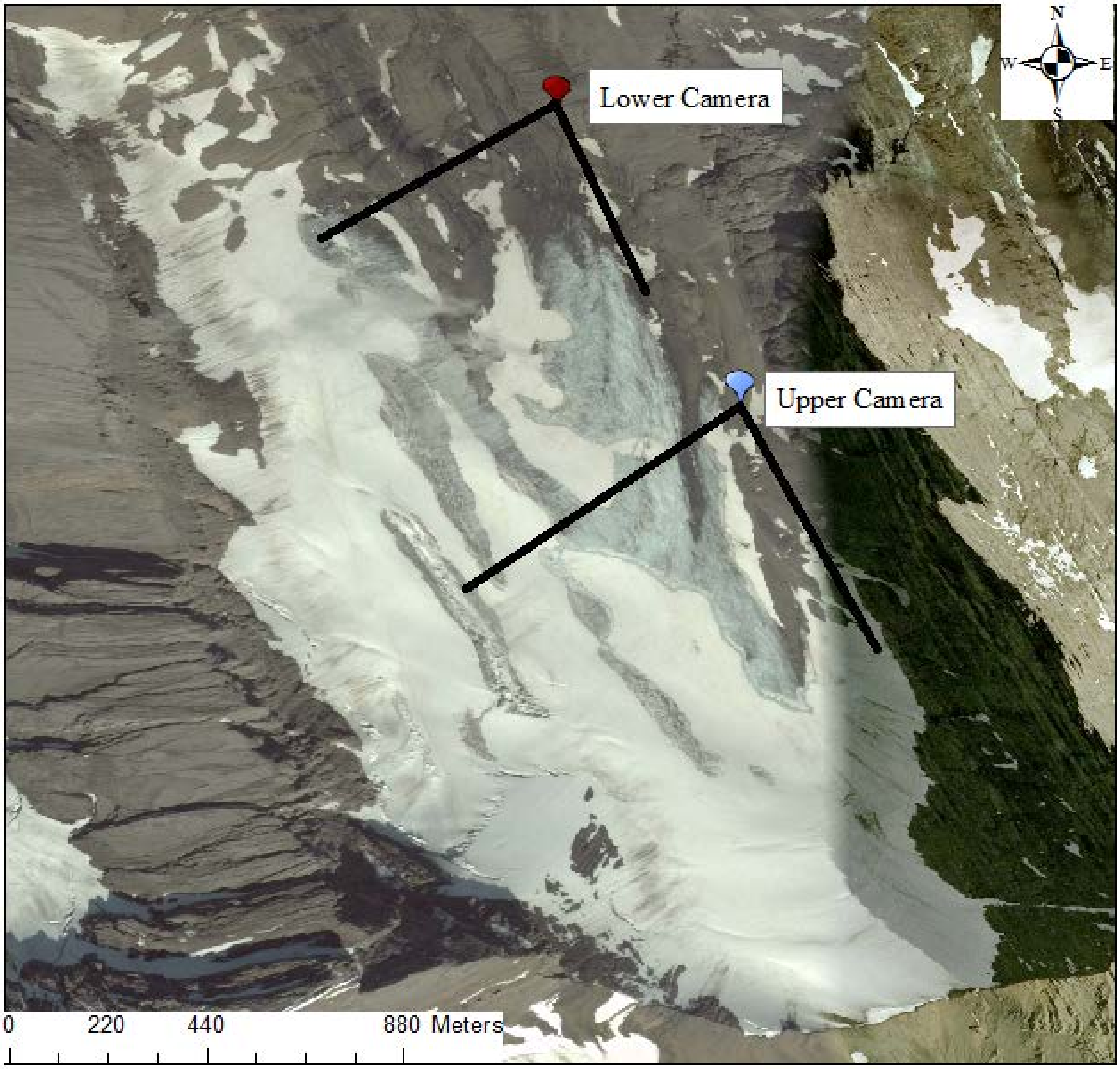

Figure 2.5. Location of time lapse cameras at Robertson Glacier, showing the field of view for each camera (Google, 2016).

Historic Temperature Data

A 100-year (1912-2012) temperature dataset for Robertson Glacier was required to run DD and ETI models for the glacier over the past century. Since no long-term air temperature record exists for the glacier, a modeled record was generated. The modeled dataset was generated using a combination of the air temperature records from the three data loggers on the glacier and the Robertson and Banff AWS.

Historic daily temperature records were downloaded from the National Climatic Data Center (NCDC), a division of the National Oceanic and Atmospheric Administration (NOAA), for six automatic weather stations within 100 km of Robertson Glacier. Of these six, only one station, Banff, had a continuous record dating back far enough to generate a modeled 100-year record of air temperature for Robertson Glacier. Daily air temperature averages from the Banff AWS, Alberta (51°11’36” N, 115°33’8” W), elevation 1396 meters, were downloaded for 15 May 1912 –15 October 2012 (Figure 2.6). From this data, a modeled record for air temperature was created for Robertson Glacier using a simple linear regression between the Banff AWS and the data loggers that were deployed on the glacier during the 2012 melt season. The simple linear regression was performed using the statistical package R, the code can be found in Appendix A. Environmental lapse rates were also calculated between the Banff AWS and the AWS in the Robertson Glacier catchment (2062 m), hereafter “Robertson AWS”, and the data loggers deployed on the glacier during the melt season of 2012. The lapse rates were calculated by taking the temperature difference between two locations and dividing by the elevation difference. This was done for the combination all loggers, Robertson AWS, and Banff AWS daily. A summary of the lapse rate combinations that were calculated is shown in Table 2.3.

Table 2.3 Lapse rates calculated for the combination of all loggers, and the two AWS, Robertson and Banff.

	Banff	**Robertson**	**2504 m**	**2642 m**	**2866 m**
Banff		X	X	X	X
Robertson			X	X	X
2504 m				X	X
2642 m					X

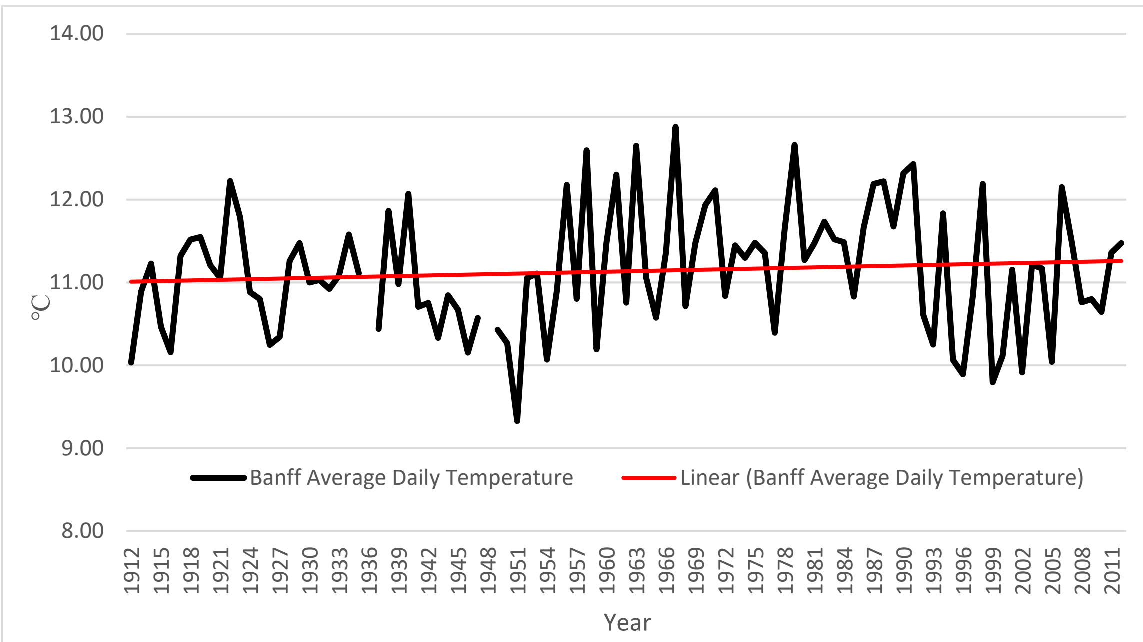

Figure 2.6. Average Daily Temperature at Banff for period 15 May-15 Oct from 1912-2012. Linear trendline is shown in red.

Historic Snowfall Data

The input variable, snow, must be calculated or approximated to calculate mass balance. Historic annual snowfall in this study was approximated using ClimateAB software (Alberta Environment, 2005; Mbogga et al. 2010). Per Mbogga et al. (2010), this computer program can calculate 36 climate variables, including annual precipitation as snow, based upon a variety of interpolation techniques, including kriging and neural networks after Attore et al. (2007), thin plate splines after Hutchinson, (1995) and Parameter Regression of Independent Slopes Model (PRISM) after Daly et al. (2002). The data quality from this software changes over time for the whole of Alberta. Data in the first half of the 20th century contains errors of 25% in one out of five years due to poor weather station coverage, while errors in the second half of the century are within 15% (Mbogga et al. 2010).

The inputs required to use ClimateAB are: Latitude, Longitude, elevation, and time frame (Figure 2.7). Thirty-six outputs are available; however, for this study the only one of interest was annual precipitation as snow (PAS). Latitude, Longitude, and elevation data from the glacier terminus (2386 m) and from the col (2866 m) were used to generate an annual record of precipitation as snow for these two locations dating back to 1912, concurrent with the modeled air temperature record.

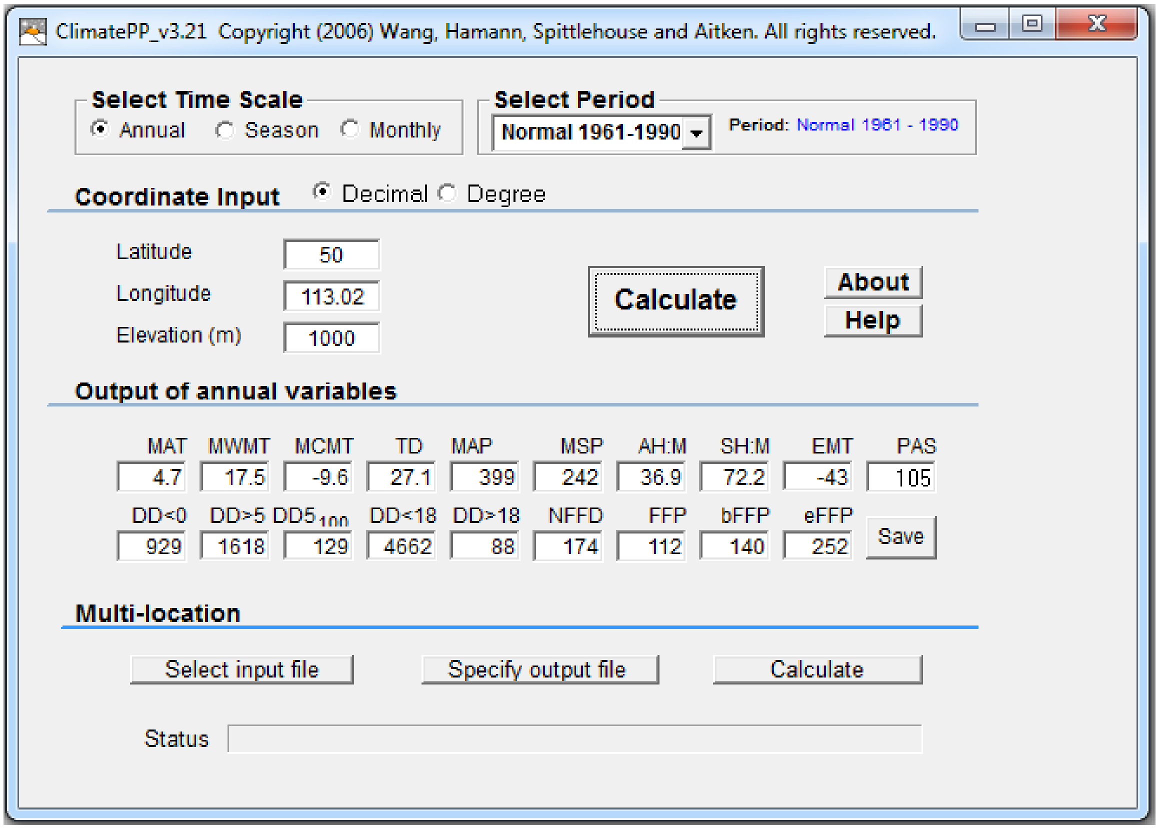

Figure 2.7. Dialogue window for ClimateAB (Alberta Environment, 2005).

<u>Albedo Calculation</u>

Albedo is the proportion of incoming solar radiation that is reflected, divided by the total incoming solar radiation (Cuffey & Paterson, 2010). There is a wide variance in albedo values that can occur within different surface types for glacier/snow surfaces (Table 2.4). In this analysis surface conditions were parameterized using snowfall estimates created by the PRISM program. There were three different values used for albedo depending upon glacier conditions. Old clean wet snow, 0.60, was used for the beginning of the melt season, May 15. Once summer melt was greater than or equal to the previous year's snowfall the albedo of clean ice, 0.35, was used above 2550 m

(Figure 2.8a) and the albedo of debris-rich ice, 0.20, was used at an elevation below 2550 m (Figure 2.8b) This is due to the high amount of debris cover below 2550 m.

Table 2.4 Common albedo values (Cuffey & Paterson, 2010).

Surface Type	**Recommended**	**Minimum**	**Maximum**
Fresh dry snow	0.85	0.75	0.98
Old clean dry snow	0.80	0.70	0.85
Old clean wet snow	0.60	0.46	0.70
Old debris-rich dry snow	0.50	0.30	0.60
Old debris-rich wet snow	0.40	0.30	0.50
Clean firn	0.55	0.50	0.65
Debris-rich firn	0.30	0.15	0.40
Superimposed ice	0.65	0.63	0.66
Blue ice	0.64	0.60	0.65
Clean ice	0.35	0.30	0.46
Debris-rich ice	0.20	0.06	0.30

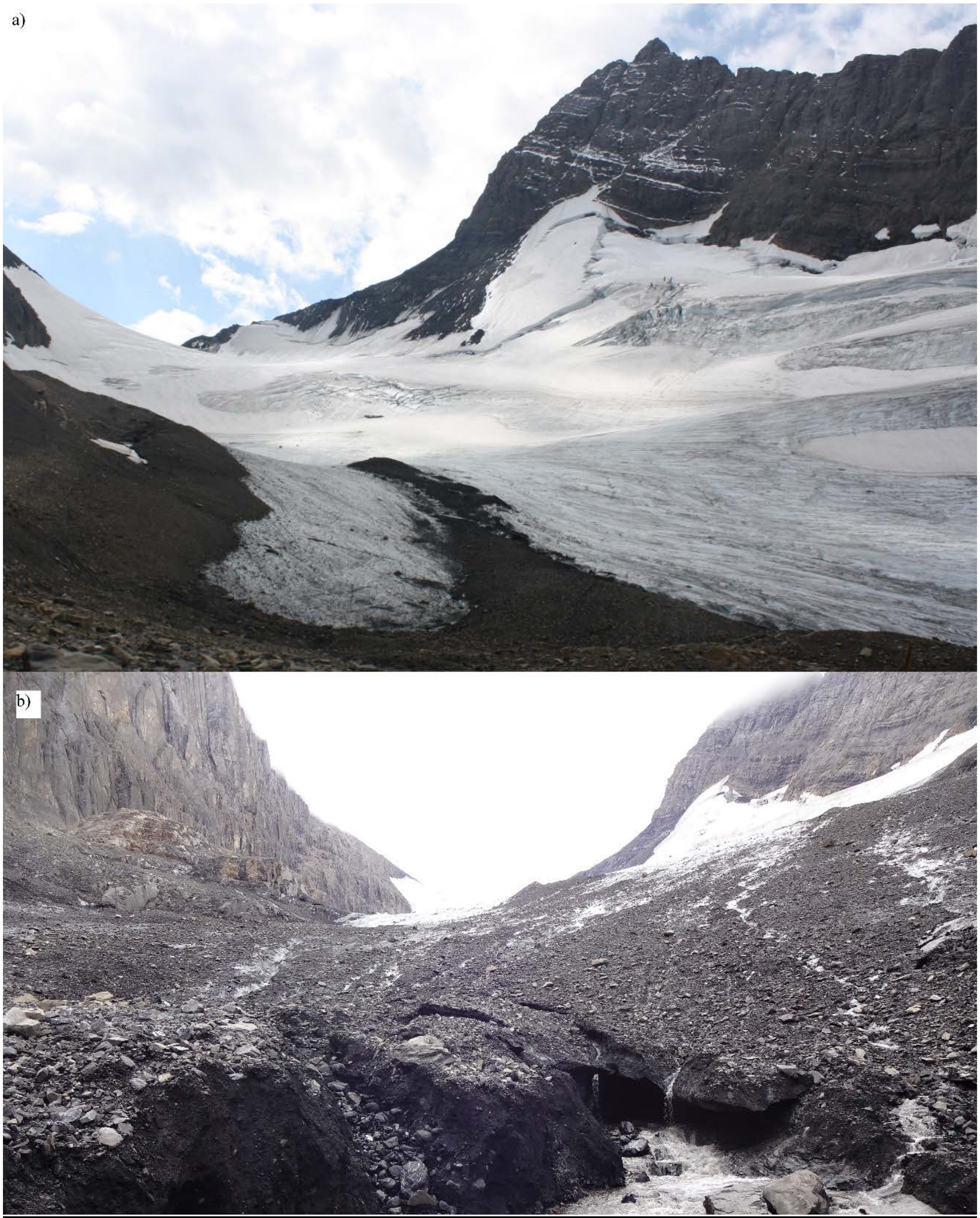

Figure 2.8 Different glacier cover types for albedo parameterization. 2.8a shows clean ice on the glacier above 2550 m. 2.8b shows heavily debris covered ice below 2550 m. Photos taken looking south.

Incoming Solar Radiation Calculation

Numerous studies have found that shortwave solar radiation is the dominant source of melt energy for most glaciers (e.g. Braithwaite & Olesen, 1990; Braithwaite, 1995; Greuell & Smeets, 2001; Willis et al, 2002). Incoming solar radiation was calculated using the measured value of solar radiation at the Robertson AWS and the clear sky value calculated in ArcGIS, a sky size of 10,000 grid cells and transmissivity of 0.6 were used to increase accuracy of modeled incoming solar radiation. Sky size is the resolution of the view shed, sky map, and sun map rasters that are used in the radiation calculation, ArcGIS defaults to a value of 200 grid cells, however, a higher value of 10,000 as used here, increases calculation accuracy. The downside to a higher resolution sky size is the significant increase in calculation time. A value of 0.6 was used for transmissivity and represents a clear sky condition that considers elevation from the Digital Elevation Model (DEM) determined via ArcGIS, and thus no correction for elevation is required. The DEM used in this study was acquired from Natural Resources Canada and was generated from 1994 data. The DEM has grid cells of 30 m^2 and a horizontal accuracy of the DEM is 22 meters, with a vertical accuracy of between 21 and 27 meters.

A ratio was then calculated between the radiation values recorded at the Robertson AWS and those modeled by ArcGIS on a daily time scale. This ratio took the measured value for solar radiation at the Robertson AWS and divided the clear sky value of solar radiation modeled by ArcGIS, similar to the approach of Hock (1999). This ratio was then multiplied by each grid cell of the solar radiation raster created for Robertson

Glacier daily giving an estimate of the solar radiation for each cell on the glacier for the period of 2007-2012. Ratio values were then averaged to create an average ratio for each day for the period of 1912-2006, i.e. May 15th 2007-2012 values were averaged to generate an average ratio for May 15th, 1912-2006?

Historical Glacier Surface Area Determination

Previous studies using satellite images to determine glacier area, have used LandSAT images e.g. Hendriks & Pellikka, (2007); Citterio et al. (2009); Bolch et al. (2010). LandSAT images are widely available and have a grid cell resolution of 30 m x 30m. Numerous LandSAT images were acquired for use in this study to determine historical glacier area and thus ultimately estimate ice volume. However, the resolution of the 30m x 30m grid used in LandSAT images was too large to generate accurate data on such changes due to the small area, 3.2 km^2 of Robertson Glacier and the short time difference, 1-3 years, between the images. Therefore, without accurate historical data on glacier area it was not possible to estimate glacier volumes using the LandSAT images.

Glacier Volume Calculation

Determining glacier volume is key to understanding mass balance and glacier contribution to the hydrological cycle, however glacier ice thickness is largely unknown and cannot be measured remotely (Marshall et al., 2011). Chen & Ohmura (1990) used empirical volume data from 63 glaciers around the world to derive a relationship between glacier area and volume:

$$V = cA^{\gamma} \tag{5}$$

where V (km^3) is the volume and A (km^2) is the surface area of the glacier. The constants c and γ are 0.0285 and 1.357 respectively. These values are generated from glaciers distributed worldwide and are therefore considered global averages (Marshall et al., 2011). Marshall et al. (2011) used data from glaciers in North America to determine specific values of 0.0308 and 1.405 for c and γ respectively when applying this model to other North American glaciers, and these are the values used in this study.

Modeling

Mass Balance Calculation

Degree day factors (DDF) can vary greatly based upon mean temperature, albedo and turbulence (Braithwaite 1995) and location throughout the world. The lowest DDF values occur for snow covered surfaces, due to a higher albedo of snow compared to ice (Hock, 2003). Arendt & Sharp (1999) calculated a small DDF for snow covered surfaces of 2.7 mm w.e. $°C^{-1}$ day^{-1} at John Evans Glacier, Canada, 79^{o}N, while Pellicciotti et al. (2005) calculated a much larger DDF for snow cover of 7.68 mm w.e. $°C^{-1}$ day^{-1} at Haut Glacier d'Arolla, Switzerland, 45^{o}N. DDF for ice cover can vary from 5 mm w.e. $°C^{-1}$ day^{-1} at Haig Glacier, Alberta, Canada (Marshall, 2005; Cuffey & Paterson, 2010) to 16.9 mm w.e. $°C^{-1}$ day^{-1} at Khumbu Glacier, Nepal (Kayasthaet al. 2000). DDF are broadly a function of latitude and values from various glaciers and ice sheets around the world are shown in Table 2.5.

Table 2.5 DDF values (mm w.e. °C^{-1} day^{-1}) for various locations, worldwide. These values are sorted based upon latitude.

Location	DDF Snow	DDF Ice	Latitude	Altitude (m, a.s.l.)	Source
Arctic					
Qamanârssŭp sermia, West Greenland	2.8	7.3	64°28'N	370-1410	Jóhannesson et al. (1993)
Qamanârssŭp sermia, West Greenland	3.7	8.3	64°28'N	790	Braithwaite, (1995)
Nordbogletsher, West Greenland	2.9	8.1	61°28'N	880	Braithwaite (1995)
North Greenland		5.9-9.8		380-540	Braithwaite et al. (1998)
Arctic Canada		6.3±1.0	80°N		Braithwaite, (1981)
John Evans Glacier, Canada	2.7-5.5	5.5-8.1	79°40'N	260-1180	Arendt & Sharp (1999)
Sub-Arctic					
Supphellebreen, Norway		6.3	61°30'N	720-1740	Orheim, (1970)
Spitsbergen		13.8	80°N	310-410	Schytt, (1994)
Ålfotbreen, Norway	4.5	6	61°45'N	850-1400	Laumann & Reeh (1993)
Nigardsbreen, Norway	4.4	6.4	61°41'N	300-2000	Johannesson et al. (1995)
Nigardsbreen, Norway	4	5.5	61°41'N	300-2000	Laumann & Reeh (1993)
Hellstugubreen, Norway	3.5	5.5	61°34'N	1450-2200	Laumann & Reeh (1993)
Sátujökull, Iceland	5.7	7.7	65°N	800-1800	Johannesson et al. (1995)
Storglaciaren, Sweden	3.2	5.4-6.4	67°55'N	1250-1550	Hock (1999)
Mid Latitude					
Haig Glacier, Canada		5	50°N	2700	(Cuffey & Paterson, 2010; Marshall, 2005)
Aletschgletsher, Switzerland	5.5		46°27'N	3366	Lang (1986)
Glacier de Sarennes, France	3.8	6.2	45°5'N		Vincent & Vallon (1997)
Griesgletscher, Switzerland		8.3-9.4	46°26'N		Braithwaite & Zhang (2000)
Haut Glacier d'Arolla, Switzerland	7.68	10.8	45°59'N	2800-3000	(Pellicciotti et al., 2005)
Perito Moreno, Patagonia, Argentina		6.9-7.1	50°28'S	330	Takeuchi et al. (1996)
Khumbu Glacier, Nepal		16.9	30°N		Kayastha et al. (2000)

DD Model Factor Calculation

Ablation totals for Robertson Glacier were calculated for the period of July 7th – August 11th 2012. This period was chosen to due to the consistency of the ablation measurements. Ablation totals were calculated in mm SWE from physical measurements at each of the three ablation stakes. This total was then divided by the total °C at each stake for the study period. This gave three different DDF values 5.13, 4.27, and 5.04, for the stakes at 2504, 2624, and 2866 m respectively, and these were averaged to give an estimate of 4.82 mm w.e. °C^{-1} day^{-1}. This is close to the average value of 5.0 mm w.e. °C^{-1} day^{-1} for the neighboring Haig Glacier, Marshall (2005), but, it is worth noting that the DDF values for both glaciers are a combination of values from a snow-covered surface and ice covered surface.

ETI Factor Calculation

ETI factors were calculated using the same period of July 7th – August 11th 2012. Ablation totals, M, total positive degree days, T, and total Wh m^{-2}, G, and albedo, α, were calculated or modeled. There are two key differences between the ETI model derived by Pellicciotti et al. (2005) and the ETI model used in this study. In the original ETI model, incoming solar radiation (G) was expressed in units of w m^{-2} and the SRF was in m^{2} mm w.e. w^{-1} hr^{-1}. In this study, incoming solar radiation (G) is in units of (Wh) m^{-2}, which are to the output units of the ArcGIS solar radiation calculator. This changes the units for the empirical constant SRF to m^{2} mm w.e. (Wh^{-1}) day^{-1}. While this unit change is not intuitive, the math correctly balances the equation, but it is therefore not possible to directly compare SRF values from Pellicciotti et al. (2005) and this study. SRF and TF values were optimized, through an iterative process using the ETI equation (5);

$$M = \begin{cases} (TF) * T + [SRF * (1-\alpha) * G] & T \leq 0℃ \\ 0 & T \leq 0℃ \end{cases} \tag{5}$$

Linear regression was then applied to the measured ablation data and modeled data. Numerous combinations of SRF and TF values were used to generate the highest regression coefficient (R^2), and the results of the optimal linear regression are shown in Figure 2.9. The value for TF is 2.06 mm w.e. day^{-1} °C^{-1} and the value for SRF is 0.01 m^2 mm w.e. (Whr^{-1}) day^{-1}.

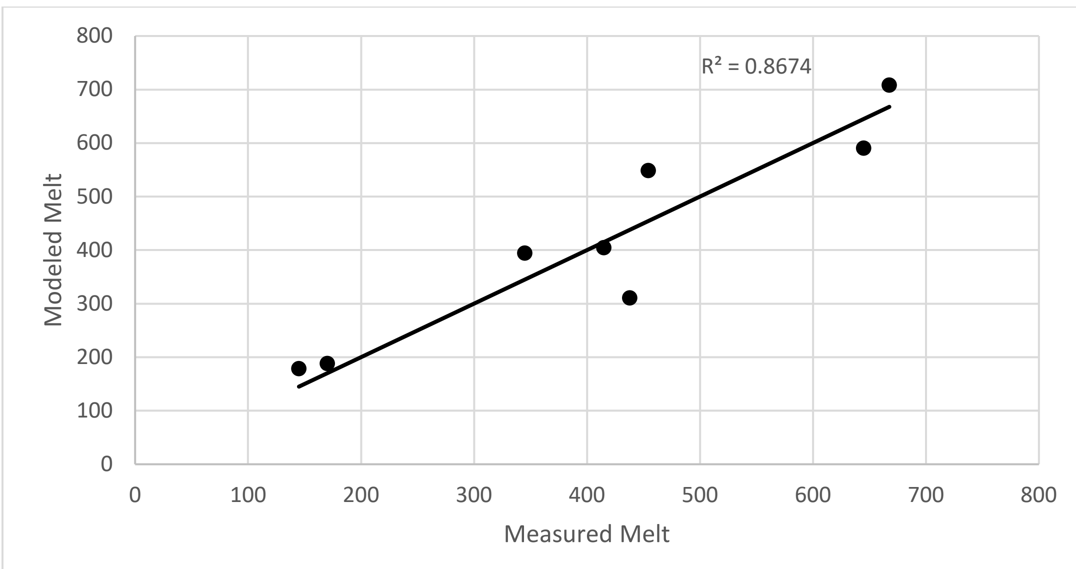

Figure 2.9 ETI Factor Calculation. The R^2 is 0.87 with the equation of the line being y=x.

Model Design

The DD model only considers elevation and corresponding temperature, as shown in Figure 2.10. T_1, T_2, and T_3 correspond to daily average air temperature collected at loggers at 2504 m, 2642 m and 2866 m respectively while the DEM raster and DDF are held constant throughout the year. This process generates a daily melt raster. These daily rasters are then summed for the period May15 to October15 and modeled snowpack data generated from ClimateAB is subtracted producing a raster that models annual mass loss, these annual mass loss rasters were also combined into decadal rasters.

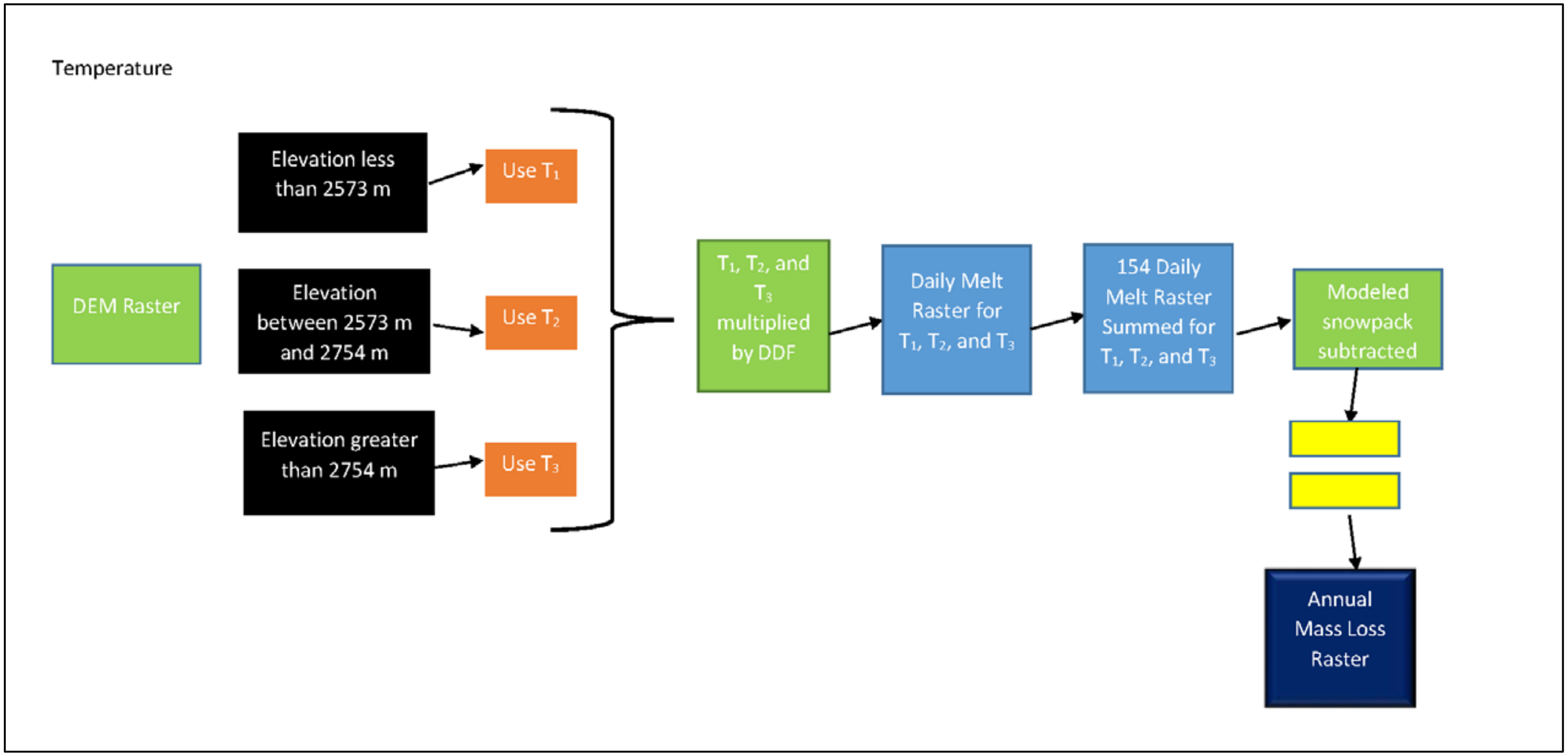

Figure 2.10. DD Model Flow Chart. T_1, T_2, and T_3 are modeled daily for the period May 15-October 15. The DEM raster for the glacier is fixed as is the DDF. This generates a daily melt raster which are then summed for the melt season and the modelled snowpack data is subtracted. This results in a raster being created that shows annual mass loss.

A schematic of the design for ETI model is shown in Figure 2.11. The model considers the differing values of albedo based on melt and elevation, the temporal variation of shortwave radiation, and the spatial variability of temperature due to elevation, as outlined above. T_1, T_2, and T_3 correspond to daily average air temperature collected at loggers at 2504 m, 2642 m and 2866 m respectively. The ETI model generates a melt raster for one day, and 154 melt rasters are calculated for each melt year, 15 May-15 October. These 154 rasters are then combined into one melt raster for each year. Modeled snowpack is then subtracted from this melt raster to create a mass loss raster for each year, which then gives an annual value in mm w.e, these annual mass loss rasters were also combined into decadal rasters.

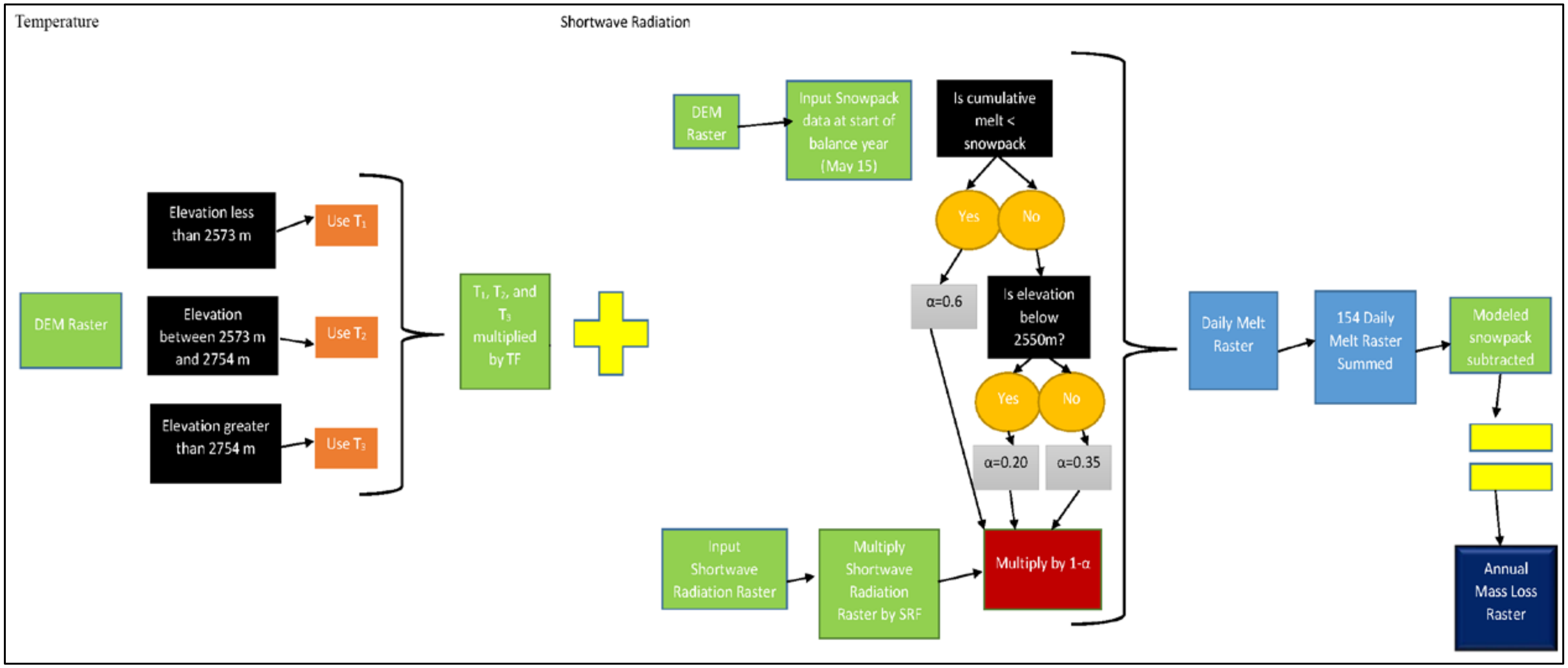

Figure 2.11. Flow Chart of the ETI model. The left side of the diagram are the calculations involving temperature and the right side are the calculations involving shortwave radiation. T_1, T_2, and T_3 are modeled daily. The DEM raster is fixed as are TF and SRF. Snowpack data is generated from ClimateAB and is based upon snowpack on May 15^{th} of each year and no snowpack data is added during the period 15 May to 15 October 15. The shortwave radiation raster varies on a daily time scale and α varies based upon cumulative melt and the snowpack. This generates a daily melt raster which is then summed for the melt season and the snowpack data is subtracted. This results in a raster being created that shows annual mass loss.

CHAPTER 3 – RESULTS

Air Temperature Data, July – September 2012

The daily average air temperature records from the three Hobo temperature loggers that were deployed on the glacier, and used in this analysis are shown in Figure 3.1a. The three loggers, deployed at elevations, 2504m, 2642m and 2866m all show similar trends in air temperature throughout the deployment period, with linear regression R^2 values of the individual temperature records all ≥ 0.92 (Table 3.1). However, the three air temperature records show small offsets, with lower temperatures at higher elevations.

Table 3.1 Linear Regression R^2 values for the air temperature records from the three loggers deployed on Robertson Glacier.

R^2	2504m	2642m	2866m
2504m		0.99	0.92
2642m			0.94

The air temperature records from the three Hobo temperature loggers on the glacier are plotted with the air temperature data from the Robertson AWS deployed down valley from the glacier at 2062m for July-September, 2012 (Figure 3.1b). Similar patterns in air temperature variability are evident for the AWS and the logger data from the glacier, with R^2 values for linear regression between the individual logger air temperature records and that from the AWS being ≥ 0.77 (Table 3.2). The AWS air temperature record is on average offset by 3.1°C relative to the logger record at 2504m, being warmer due to the lower elevation of the Robertson AWS, while the offset is on average 3.0°C between the air temperature data recorded at the Banff AWS and the

Robertson AWS, with the Banff data showing warmer temperatures. The correlation between the air temperature records from the Robertson AWS and the data logger records is stronger for the lower elevations on the glacier (2504m, 2642m) than for the highest elevation (2866m) (Table 3.2).

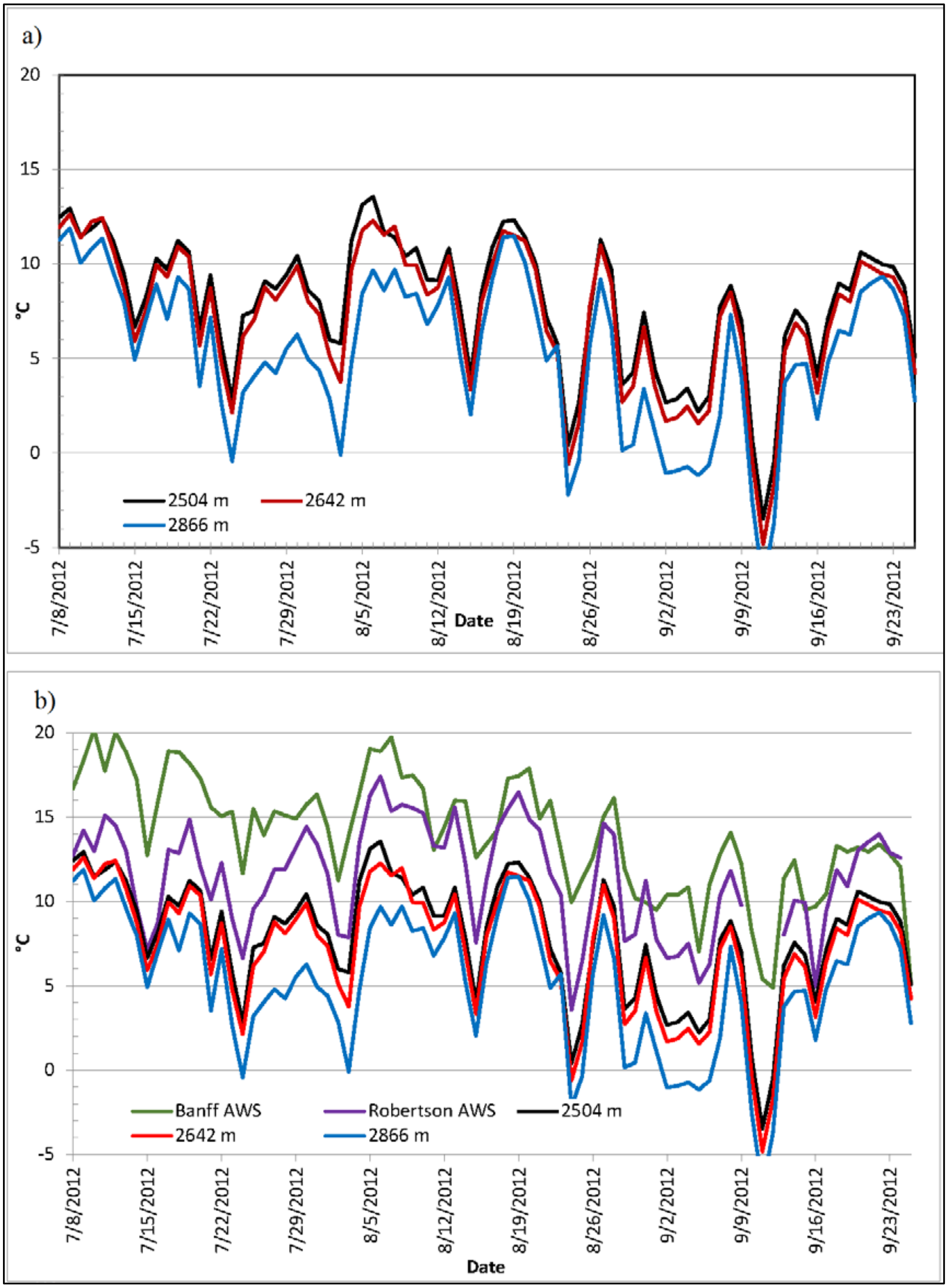

Figure 3.1. a): Daily average air temperatures recorded by the three Hobo loggers on Robertson Glacier. b) Daily average air temperatures recorded by three Hobo loggers, and the Robertson AWS and Banff AWS. Elevations of the loggers are shown in the legend.

Table 3.2 R^2 values for the air temperature records from the three loggers deployed on the glacier compared to the Robertson AWS and Banff AWS air temperature records.

R^2	2504m	2642m	2866m
Robertson AWS	0.88	0.88	0.77
Banff AWS	0.71	0.71	0.63

There is short data gap in the Robertson AWS temperature record from 10^{th}-11^{th} September (Figure 3.1b). Here, the Robertson AWS record showed temperatures that were 28°C lower than the logger at 2504m. There was a significant snow storm that occurred on the 10^{th} and 11^{th} of September but it is unlikely though that this would cause such a temperature disparity within an elevation range of 355 m and therefore this data likely reflects a sensor malfunction at the Robertson AWS. The Robertson AWS temperature data also shows a similar ~ 30^{o}C rapid decrease in in early July 2012, also associated with a significant snow storm. This data is also considered to be due to a similar sensor malfunction and has been omitted from the seasonal records of air temperature shown in Figure 3.1b.

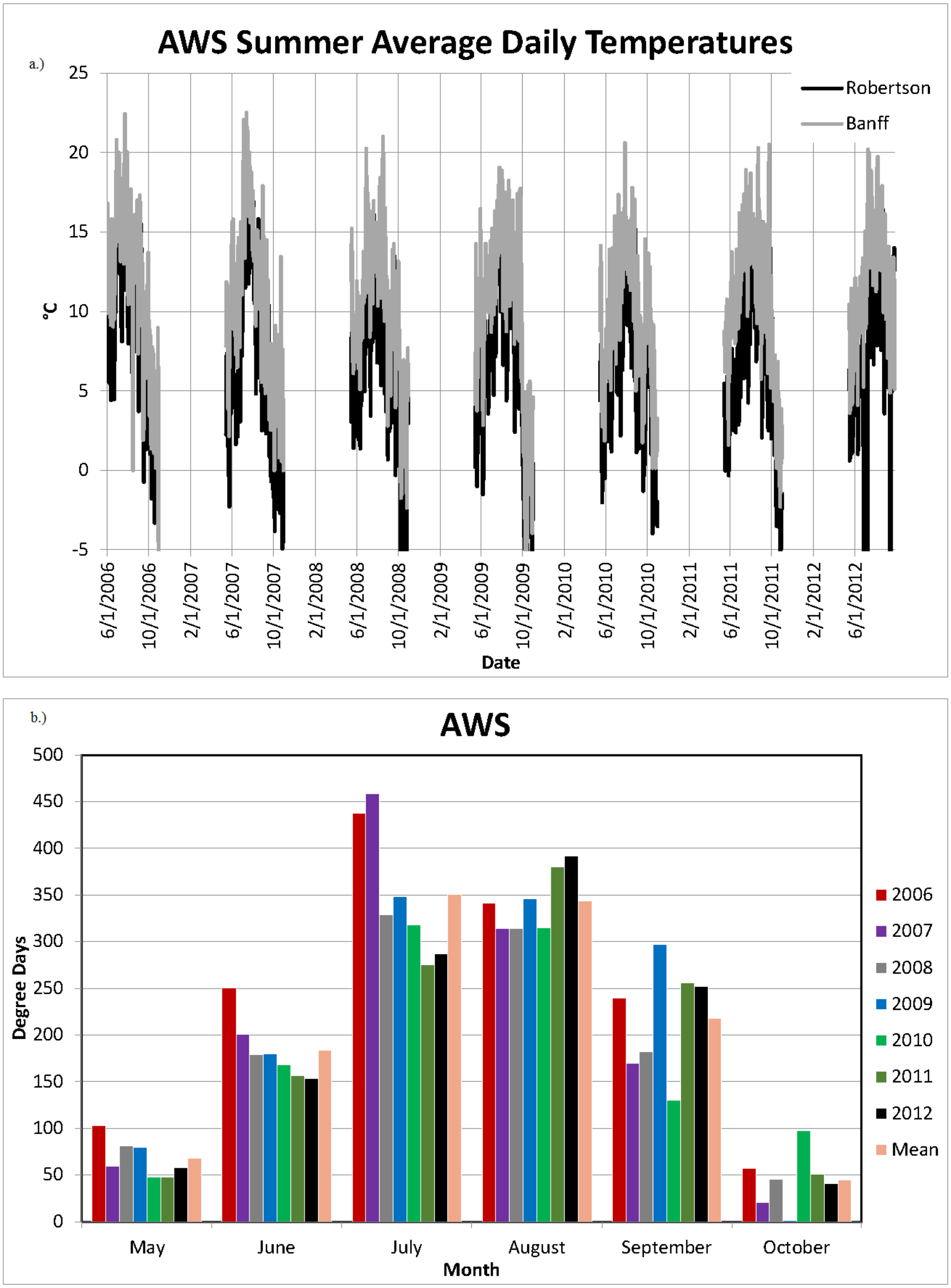

Figure 3.2. a) Robertson AWS and Banff AWS average daily air temperature records 15 May-15 October, 2006-2012. b) Degree day totals and means by month for 2006-2012 at the Robertson AWS.

Air Temperature Data 2006-2012

Summer average daily air temperatures recorded at the Robertson AWS and the Banff AWS are shown in Figure 3.2a. The same general inverse parabolic shape in air temperature is evident for each of the six summer seasons. The total degree days for each summer at the two sites are shown in Table 3.3. The Robertson AWS had lower degree day totals for each year than the Banff AWS, with the mean being 532 days lower, but the Robertson AWS showed greater variability in degree days than the Banff AWS, over the seven-year period (c.v. = 10.7% relative to 4.9%) (Table 3.3). The difference in degree day means reflects the temperature change due to elevation. The standard environmental lapse rate is estimated to be 6°C/1000m (Oke, 2002), however, for the elevation change between the Robertson AWS and Banff AWS (676m), the mean temperature difference is 3°C, which corresponds to a lapse rate of 4.4°C/1000m (see Figure 3.1b), and is therefore lower that the standard environmental lapse rate.

Table 3.3 Degree Day totals for the Robertson AWS and Banff AWS, for 2006-2012. The means, standard deviation (s.d.) and coefficient of variance (c.v.) are also shown.

Year	**Elev (m)**	**2006**	**2007**	**2008**	**2009**	**2010**	**2011**	**2012**	**Mean**	**s.d.**	**c.v. %**
RG DD	2062	1275	1071	977	1099	923	1013	1029	**1055**	**113**	**10.7**
Banff DD	1386	1719	1616	1508	1570	1483	1596	1616	**1587**	**78**	**4.9**

The summer with the fewest positive degree days at both stations was 2010, while the summer with the highest positive degree day totals was 2006. In 2006, the two stations exhibited the lowest difference in positive degree days, 444, with the greatest difference being in 2011, 583 positive degree days.

Figure 3.2a illustrates the correlation between the daily average air temperature data at the Robertson AWS and the Banff AWS, with a corresponding R^2 of 0.87. The monthly degree day totals and means for 2006-2012 for the Robertson AWS are shown in Figure 3.2b. For the time period measured, July has the highest number of degree days on average (350) relative to August (340), but the variability for degree days in August is much lower, which is consistent with the data from the Banff AWS.

Snowfall Data

The modeled annual snowpack for 1912-2012 at 2866m on Robertson Glacier (the highest elevation recording site for air temperature) using ClimateAB software is shown in Figure 3.4. Snowpack data was generated with the ClimateAB v3.21 software package, available at *http://tinyurl.com/ClimateAB,* based on methodology described by Alberta Environment, (2005) and Mbogga, et al. (2010). The average annual value for the snowpack over the century is xx mm SWE. A 10-year average and upper and lower bounds of one standard deviation are also shown in Figure 3.3. Notable years when the modelled snowpack greatly exceeded the one standard deviation threshold, were 1932, 1933, 1971, 1972, 1990, 1995, 1996, and 2003, whereas 1926, 1944, 1952, 1981 and 2005 were all significantly below the one standard deviation threshold.

PRISM snowpack data can underestimate that measured in mountainous regions (e.g. Jeton, 2006). Jeton et al., (2006) compared differences between PRISM estimates and observed data sets of snowpack in Nevada, with percent variance ranging from -60% to +115%. Snow pack measurements for 2640m elevation on the adjacent Haig Glacier exist for 2002 and 2003 and are substantially higher than the PRISM estimates for that location, ~ 220% greater on average (Table 3.4).

Table 3.4. Comparison of snowpack measurements and PRISM estimates for the upper elevations of the adjacent Haig Glacier and PRISM estimates for Robertson Glacier.

Year	**Robertson Glacier PRISM Estimate (2866 m) (mm w.e.)**	**PRISM Estimate Haig Glacier (2640 m) (mm w.e.)**	**Measured Haig Glacier (2640 m) (mm w.e.)**	**% Difference**
2002	637	626	1860	297%
2003	793	763	1090	143%

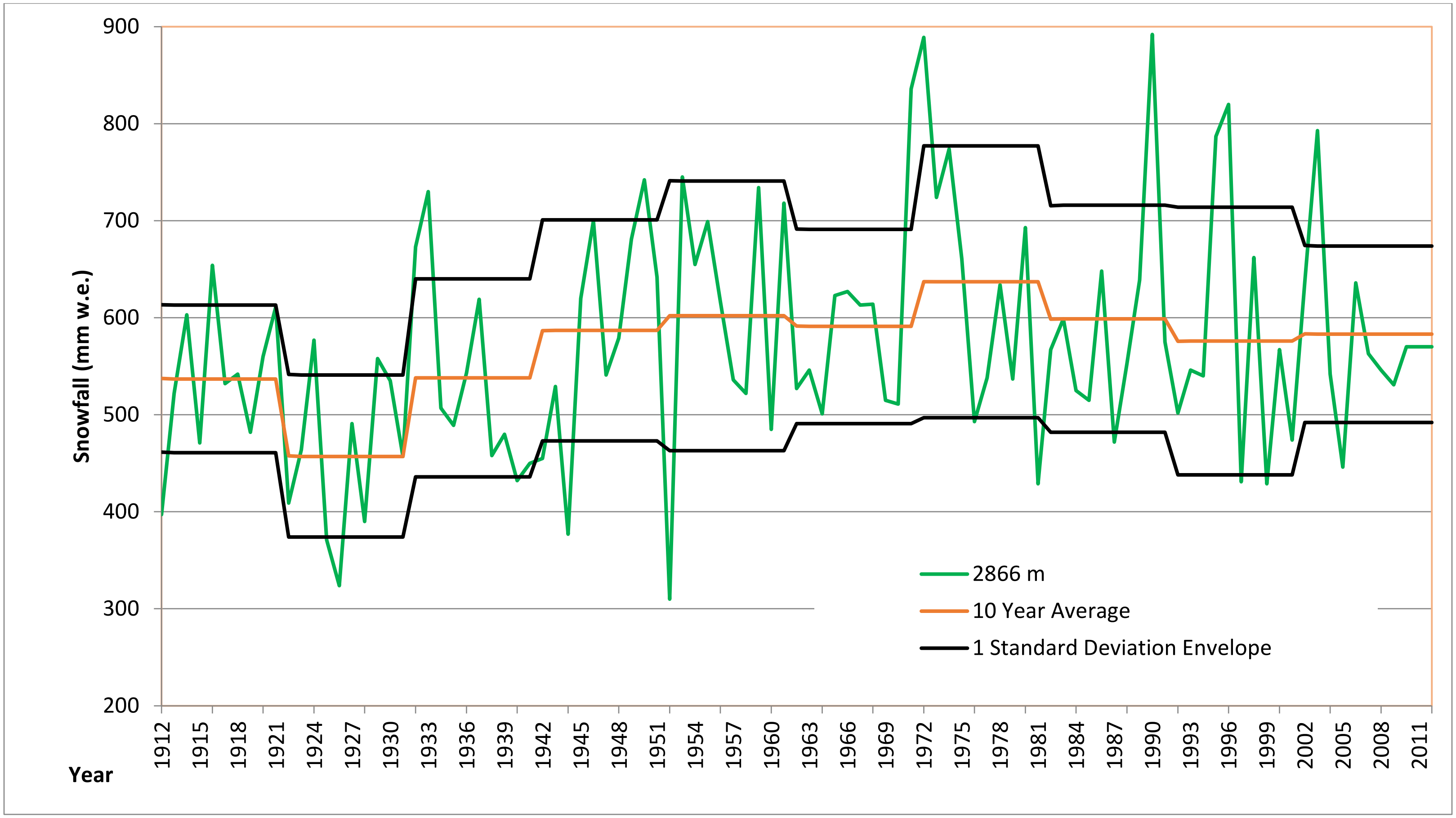

Figure 3.3. Annual PRISM modelled snowpack totals in mm w.e. for 2866m on Robertson Glacier. The ten-year mean is shown in orange with the one standard deviation upper and lower bounds relative to that 10-year average shown in black.

Modeled Temperature Record

A modeled air temperature record was created for Robertson Glacier for 1912-2012 using simple linear regression and the measured 100-year air temperature record from the Banff AWS. The R^2 values between mean daily air temperature records at the Banff AWS and glacier data loggers for July-September 2012 are shown in Table 3.2.

Linear regression between the air temperature records from the Banff AWS and each Hobo logger was done in the R statistical package and provided slope and a y-intercept with a 95% confidence interval for each of those terms (Appendix A). A simple linear regression of the air temperature records in ^{o}C between Banff and the 2504m station on the glacier produces the equation: $2504m = Banff * 0.85 - 3.97$. The 95% confidence intervals for slope and intercept are (0.73, 0.97) and (-2.2, -5.73) respectively. These 95% confidence intervals for slope and intercept provide an error envelope for the modeled temperature data record as illustrated in Table 3.5. Table 3.5, shows the average daily August air temperatures for the 2504 m elevation at twenty year intervals over the modeled record and the values for the 95% confidence intervals of slope and intercept. August was selected to conduct the sensitivity analysis as the measured air temperature data for 2006-2012 at the Robertson AWS showed the lowest natural variability during this month.

Table 3.5 Estimated mean monthly air temperatures for August at 2504m on Robertson Glacier and its variability, using the 95% confidence interval of simple linear regression between the data from the Banff AWS and logger at 2504m. All values are in ^{o}C.

August	Banff Average Air Temp	Modelled values for 2504m	2504m (Slope 97.5, Int 2.5)	2504m (Slope 97.5, Int 97.5)	2504m (Slope 2.5, Int 2.5)	2504m Slope 2.5, Int 97.5)
1912	11.6	5.9	5.5	9.1	2.7	6.3
1932	13.6	7.6	7.5	11.0	4.2	7.7
1952	12.7	6.8	6.6	10.1	3.5	7.1
1972	16.1	9.7	9.9	13.4	6.0	9.6
1992	12.7	6.8	6.6	10.1	3.5	7.1
2002	12.0	6.2	5.9	9.4	3.0	6.6
2012	14.8	8.6	8.6	12.2	5.1	8.6

A modeled record was created for the period of 1912-1922 using the lower and upper 95% confidence interval endpoints. This record was then used in the DD model to determine low and high estimates for mass loss.

Degree days were modelled for all three elevations on the glacier for 1912-2012 and show similar trends, with lower degree day totals at higher elevations; the results from 2866m are shown in Figure 3.4. The data was split into three different time periods, 1912-1957, 1958-1992, and 1993-2012, with means and one standard deviation upper and lower bounds created for these time periods, showing variability of 129, 152, and 166 DD respectively.

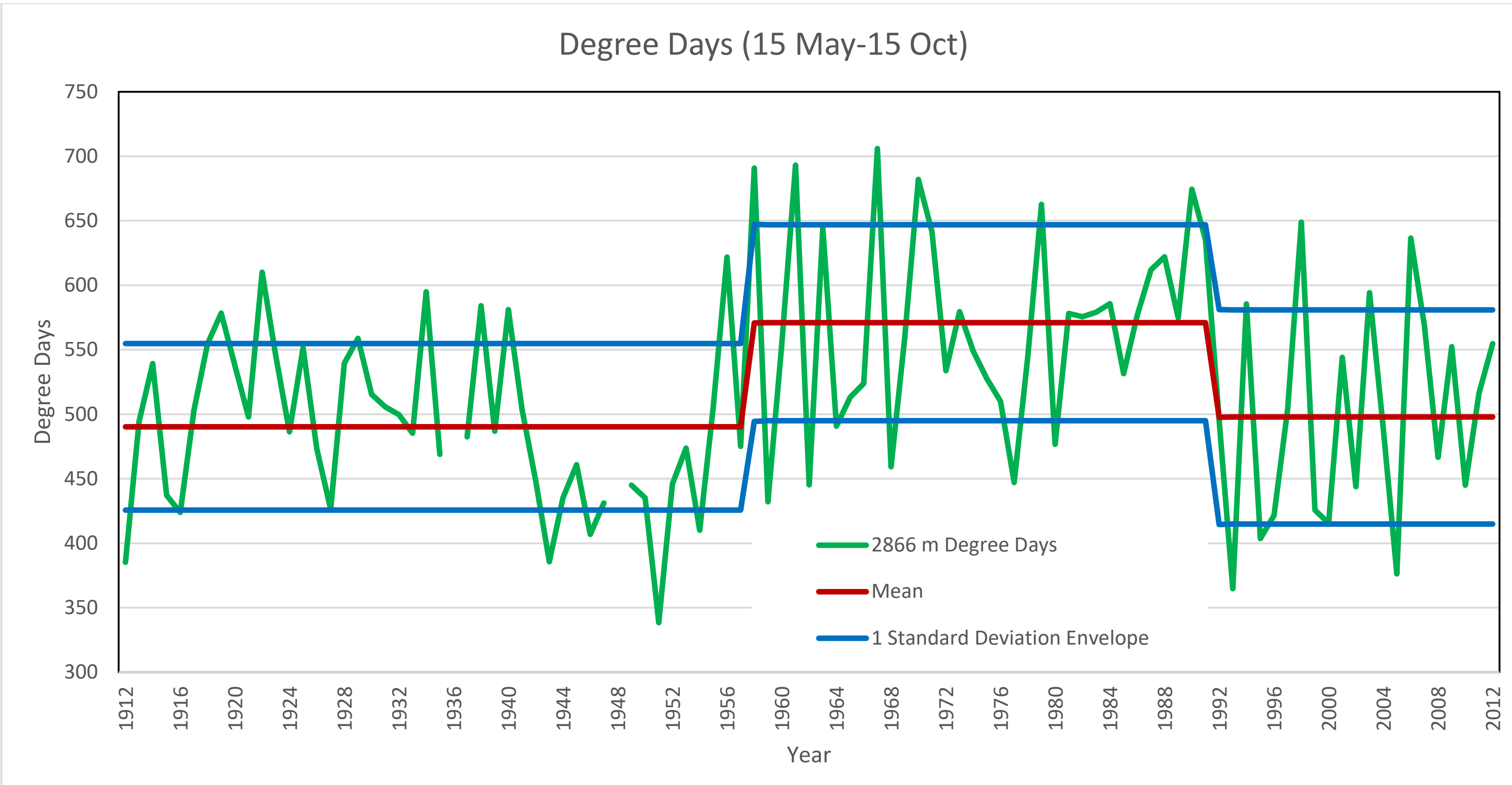

Figure 3.4. Modelled degree days for 2866m on Robertson Glacier for 1912-2012. Mean and one standard deviation error envelope shown for 1912-1957, 1958-1992, and 1993-2012.

Model Results

Mean modeled mass loss for the DD model, with a 10-year average of the means and a one standard deviation envelope is shown in Figure 3.5 (1936 and 1948 had inadequate temperature records to complete the analysis for those years). Mass loss was calculated using the DD model based upon three different elevation determined temperature bands on the glacier (Figure 3.6). The modeled mean mass loss for the glacier for the period 1912-2012 was 301 m w.e. The model output showed a significant elevation gradient in mass loss, with the highest elevation band (2754- 2861 m) showing only 191 m w.e. of mass loss with the lower bands, 2573-2754 m and 2366-2573 m, showing 312 and 360 m w.e. of mass loss respectively. Since the DDF is the same for the entire glacier these differences are based solely upon the differing temperature values for each elevation band.

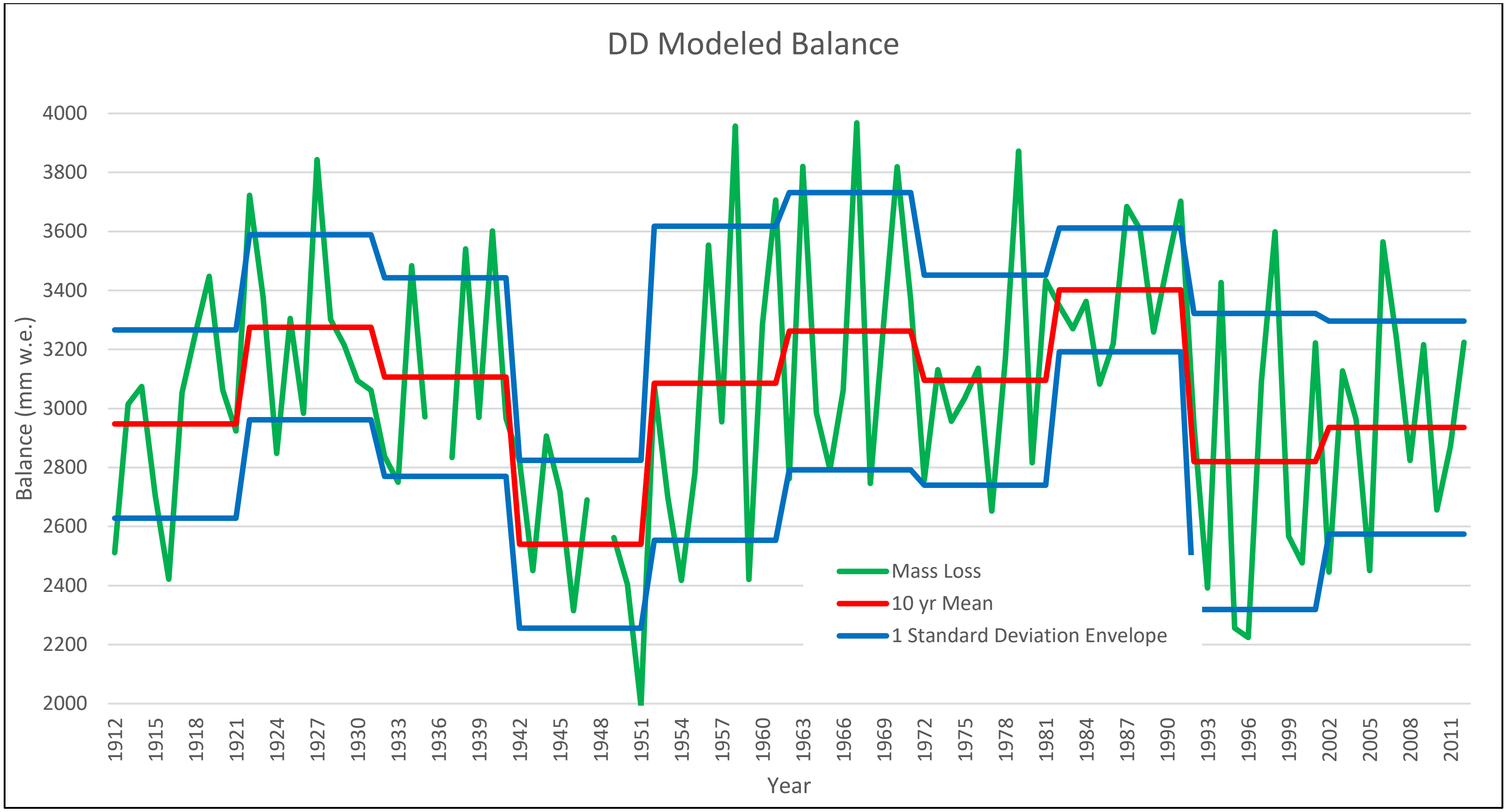

Figure 3.5. DD Modeled mass loss for Robertson Glacier with 10-year mean and one standard deviation envelope.

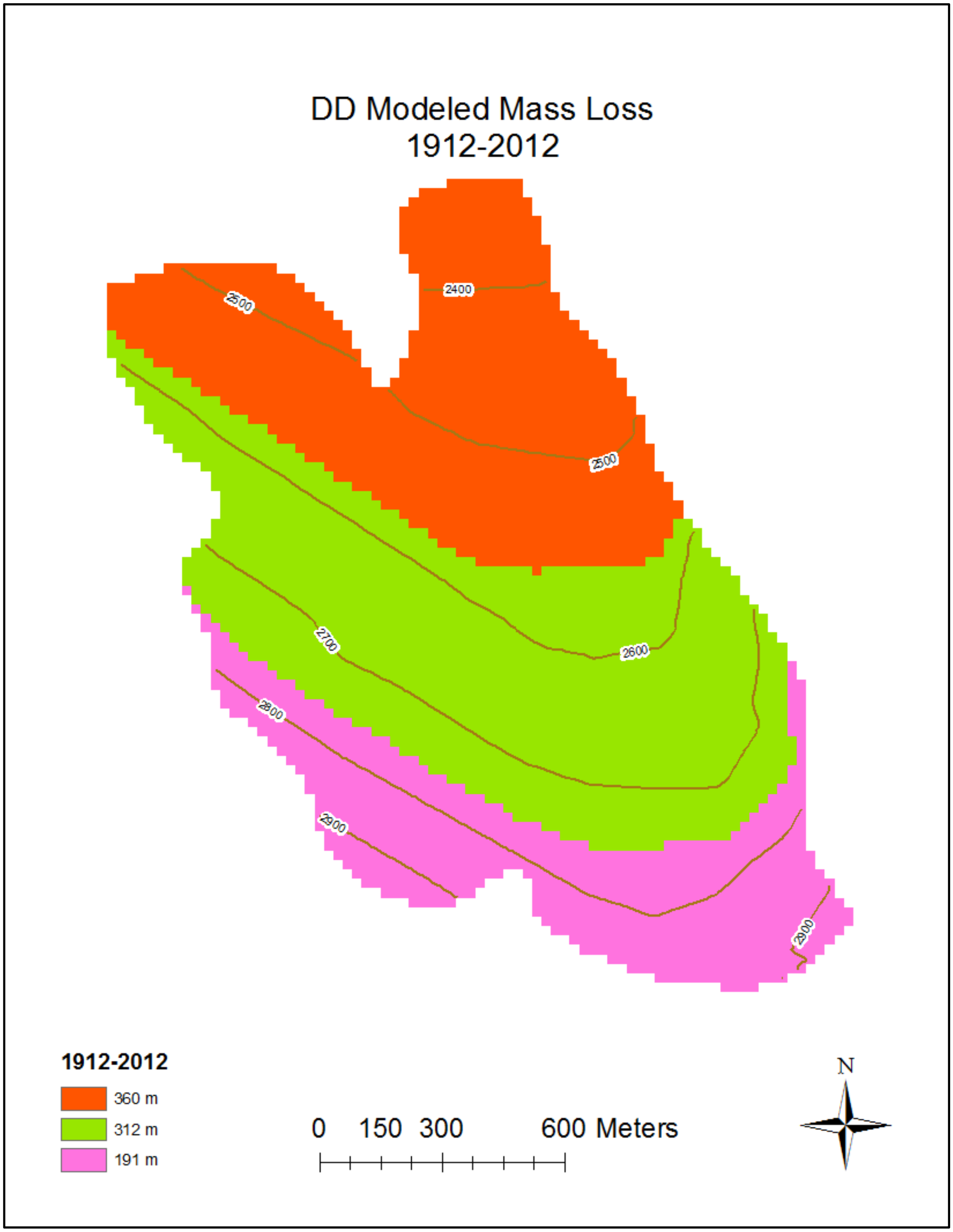

Figure 3.6. DD Modeled Mass Loss for Robertson Glacier 1912-2012 (Mass loss in m w.e.) The glacier terminus is to the north, with the orange elevation band being the lowest and the pink band the highest.

Mass loss was calculated using the ETI model for the period 1912-2012 based upon each of the 3843, 30 m x 30 m grid cells, on the glacier. Annual mean modeled mass loss using the ETI, with 10-year average of the mean and a one standard deviation envelope, (once again the years 1936 and 1948 are omitted) is shown in Figure 3.7. The modelled mean mass loss for the glacier for the period 1912-2012 was 319 m w.e (Figure 3.8). An altitudinal gradient in mass loss is also evident for the ETI model, with the highest value for a grid cell at 413 m w.e. and the lowest value of 152 m w.e. However, there is more complex pattern in mass loss, relative to that shown in the DD model, with the lowest amounts being at higher elevations, but with two regions of greater mass loss central to the glacier, circled in Figure 3.8. This pattern is based almost solely on the spatial variability of incoming and reflected shortwave radiation.

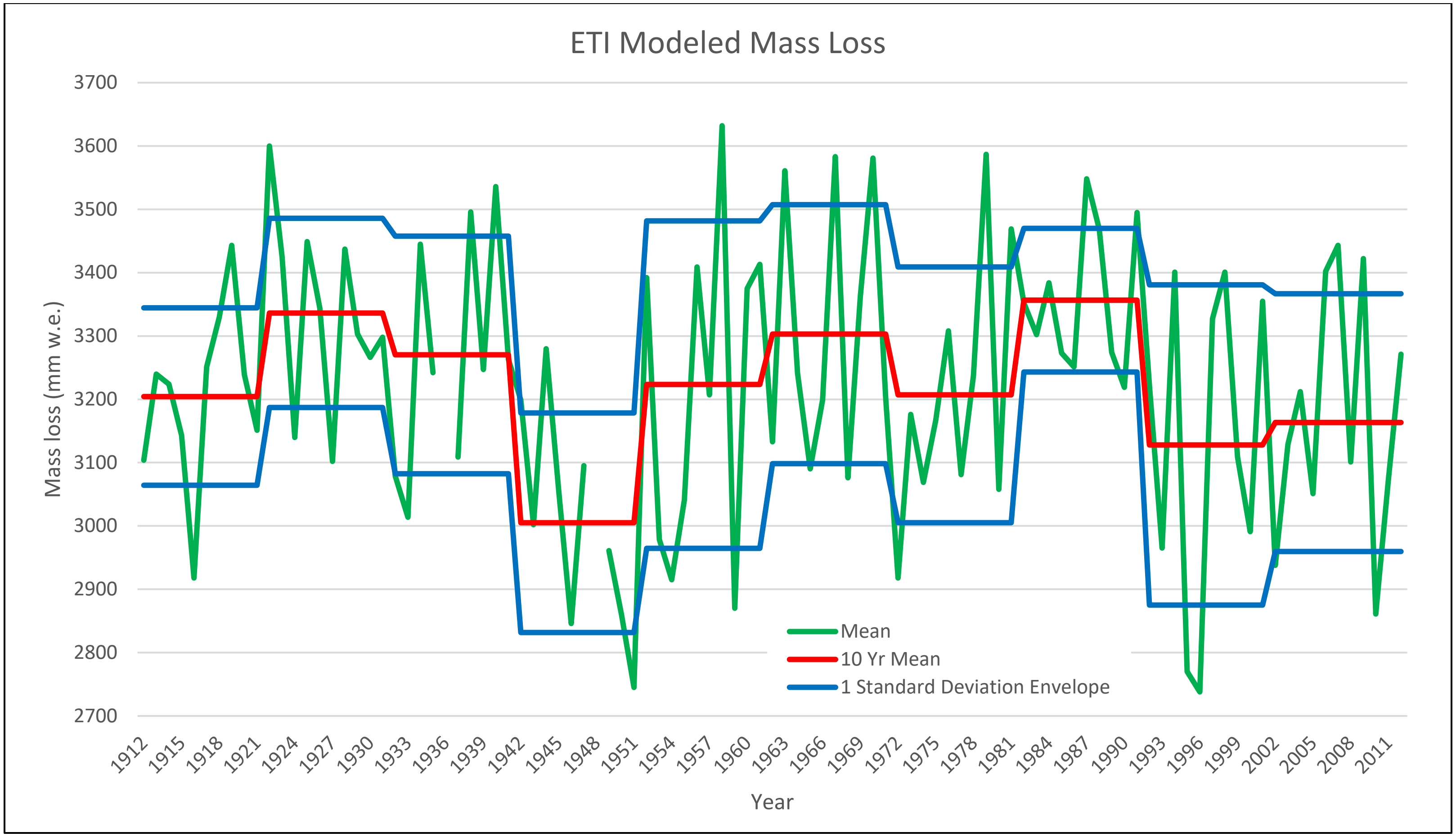

Figure 3.7. ETI Modeled mass loss for Robertson Glacier for 1912-2012 with 10-year mean and one standard deviation envelope.

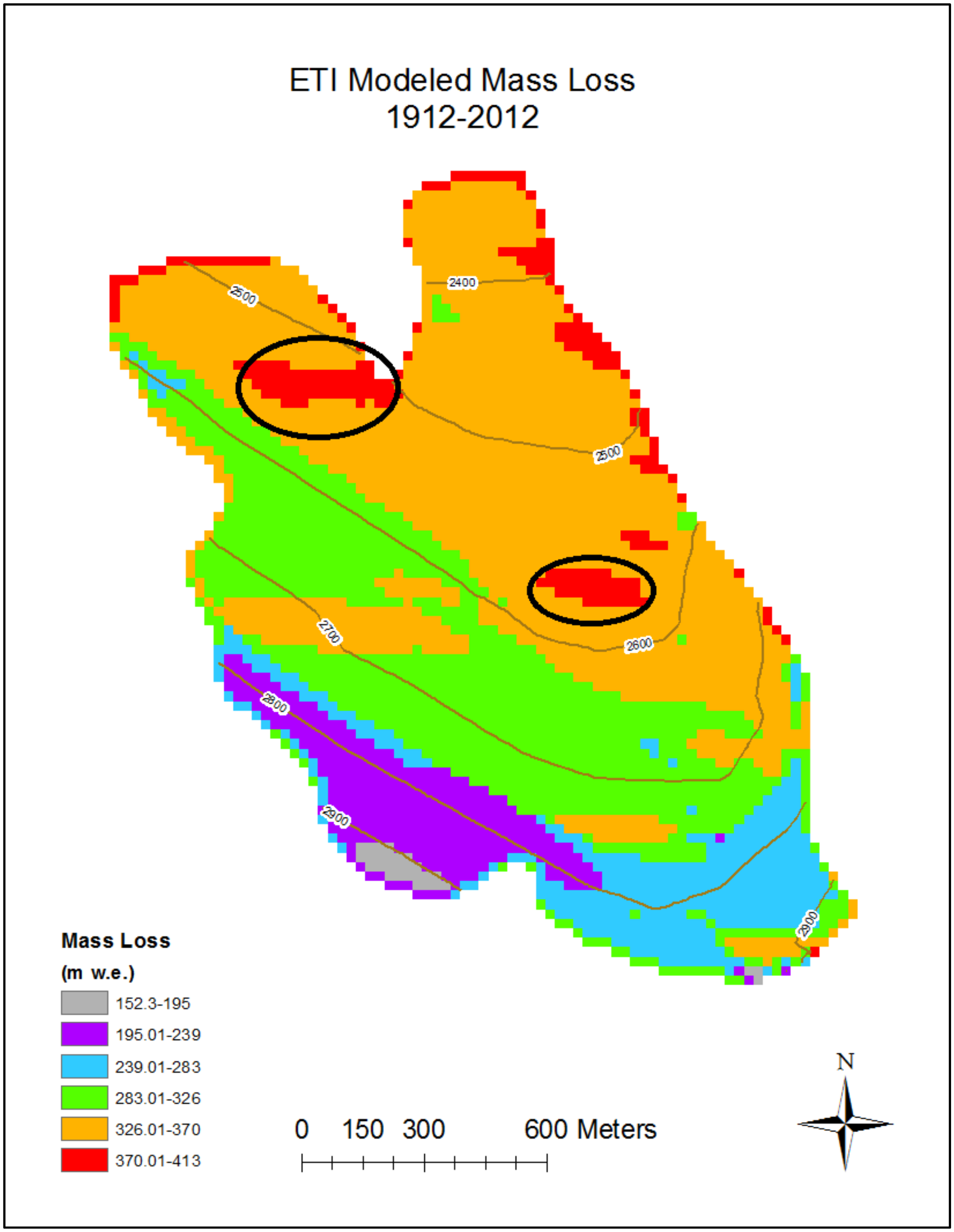

Figure 3.8. ETI Modeled Mass Loss for Robertson Glacier, 1912-2012 (Mass loss in m w.e.) Circles indicate areas of higher relative mass loss. The glacier terminus is to the north.

Model Output Comparison

The ETI model calculates 3843 values of mass loss, and showed a higher range of melt values than the DD model. The ETI had a difference of 261 m w.e. between the highest and lowest melt estimates, while the DD model had only a difference of 169 m w.e. between its highest and lowest estimated melt values. The ETI estimated more mass loss in 79 of the 99 years modeled (Figure 3.9). The greatest difference between the two model outputs was in 1951 when the ETI estimated a mass loss of 754 mm w.e. more than the DD model, while in 1967 the ETI estimated a mass loss of 385 mm w.e. less than the DD model. There is also a temporal pattern in the difference between the ETI and DD model results; three periods were identified for further analysis, 1912-1957, 1958-1992, and 1992-2012 (Figure 3.9). The ETI averaged 261 mm w.e. and 257 mm w.e. more mass loss per year than the DD model for the periods of 1912-1957 and 1992-2012 respectively, while for the period of 1958-1992 the ETI only modeled on average 29 mm w.e. more mass loss per year than the DD model. The 1958-1992 period shows higher modelled Degree Day values (Figure 3.5) and this is potentially the factor that is responsible for the average mass loss values being closer together during this period. A cumulative mass loss graph (Figure 3.10) shows a linear trend of mass loss during the period of 1912-2012 and the widening differences between estimated mass loss between the ETI and the DD models.

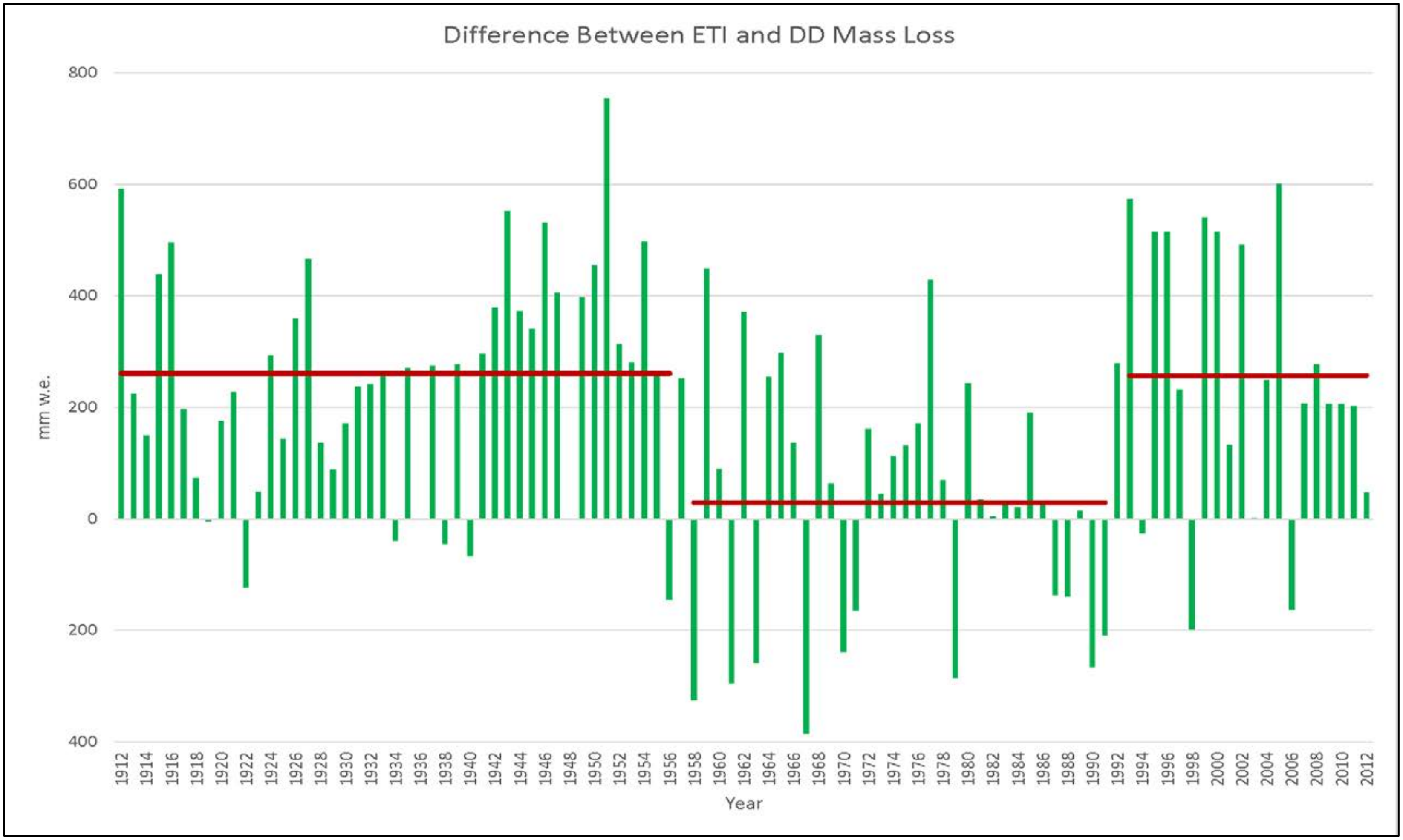

Figure 3.9. Annual difference between ETI and DD modeled mass loss for Robertson Glacier in mm w.e. Red line represents the mean difference for three periods, 1912-1957, 1958-1992, and 1993-2012.

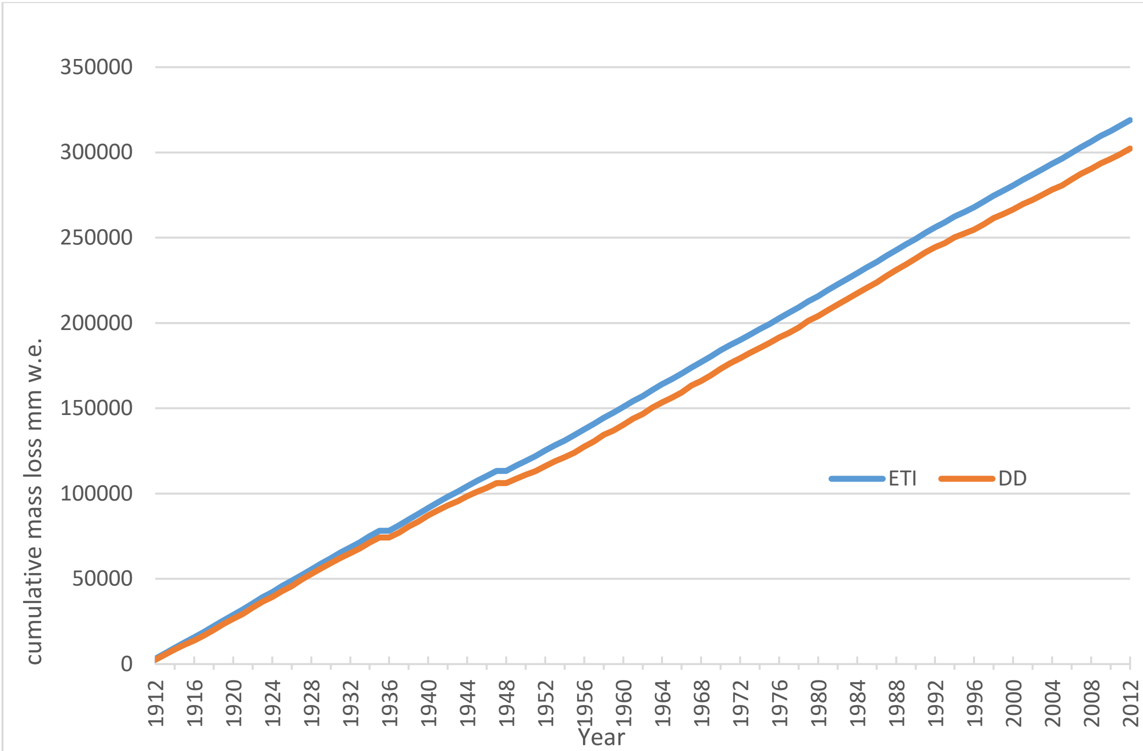

Figure 3.10 Cumulative mass loss in mm w.e. predicted by the ETI and DD models.

Glacier Volume and Estimated Future Ice Loss

The 2012 glacier volume for Robertson was calculated using the equation 5 following Marshall et al, (2011)

$$V = cA^{\gamma}$$

using the values of 0.0308 and 1.405 for c and γ respectively. This yielded an estimated average glacier thickness of 49.6 m, the estimated thickness assumes that glacier thickness is uniform, we know however from glacier dynamics and physical observations that this is not accurate. Meier et al. (2007) in their study of worldwide glaciers and ice sheets estimated an error of 50% when applying to a single glacier, however the error drops to 25% when a estimating glacier thickness regionally or globally. Radić, et al. (2008) carried out a systematic analysis of multiple glaciers throughout the world to determine how glacier disequilibrium, i.e. glaciers either retreating or advancing markedly, effects volume estimates from surface area. Radić, et al. (2008) calculated individual errors of six glaciers from different geographical locations and climatic regimes. Nigardsbreen, Norway; Rhonegletsher in the Swiss Alps; South Cascade Glacier in the North Cascades; Sofiyskiy glacier in the Russian Altai mountains; midre Lovenbreen in Svalbad and Abramov glacier in Kyrgyzstan. The largest area to volume error was 57% at Nigardsbreen (Radic et al., 2008). An average annual DD mass loss map was created for the period of 2002-2012 (Figure 3.11) and this annual loss rate was then applied to the estimated glacier thickness in 2012 to create a map indicating the estimated time when ice cover would disappear for a given elevation band, assuming all other variables are held constant (Figure 3.11). This static approach has its limitations as it does not consider ice flow. However, one might expect ice flow to accelerate the mass loss as it would be moving ice from higher to lower elevations where the rate of mass loss is greater. This estimate also does not consider the positive feedback cycle of surrounding surfaces becoming ice free and thus having a lower albedo.

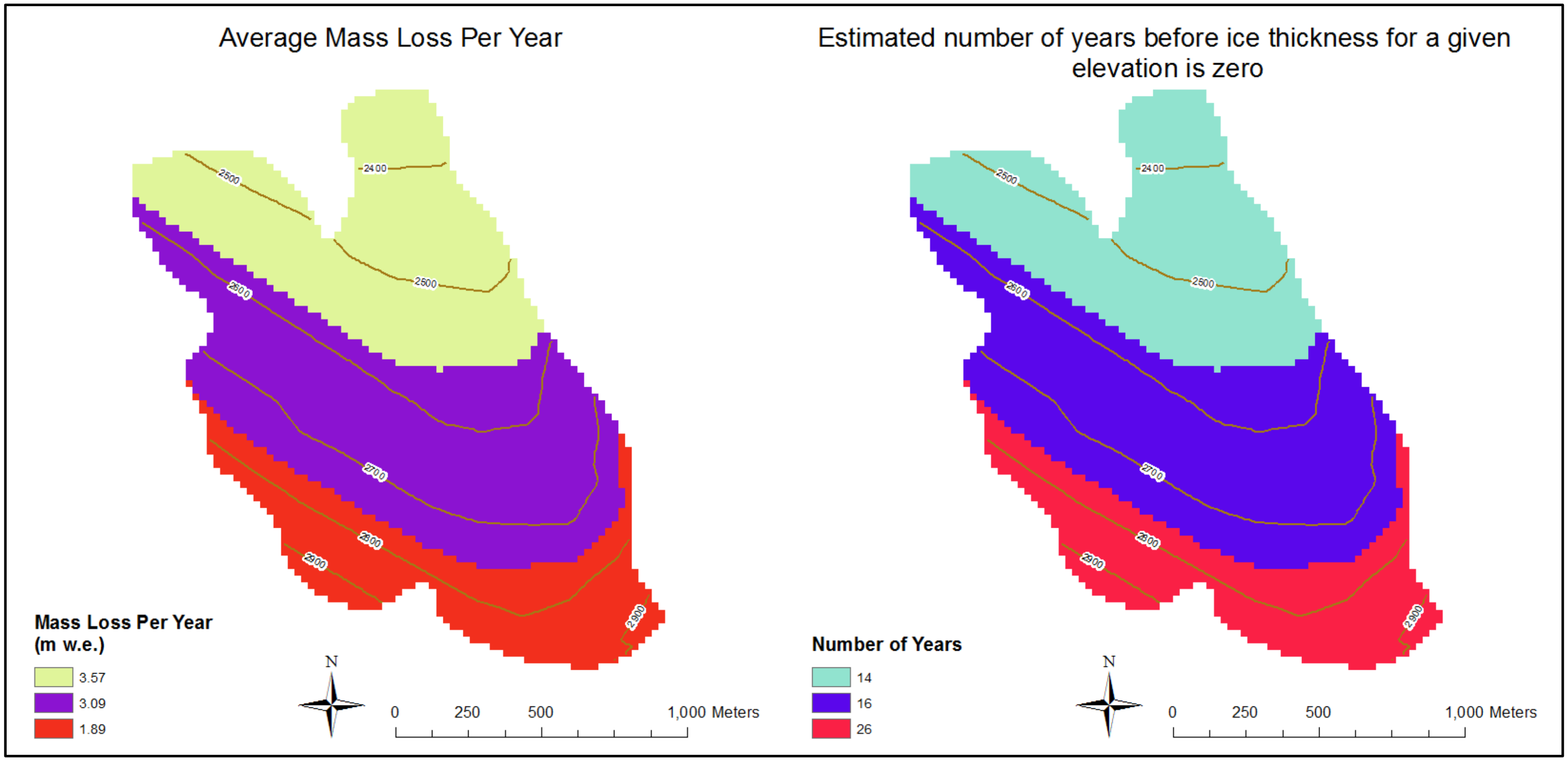

Figure 3.11. Left Panel. Estimated mass loss per year based upon 2002-2012 average daily temperatures and average annual snowpack. Right Panel. Estimated number of years before ice thickness for a given elevation is zero based upon estimated glacier thickness of 49.6 m in 2012 and applying the average mass loss per year for the period 2002-2012, forward in time. Glacier terminus is to the north.

Model Efficiency of DD and ETI Models

The DD model was run using the upper and lower endpoints of the 95% confidence interval for the modeled temperature record as described in Chapter 3 and Table 3.5 and estimates for glacier mass loss during the period 1912-1922 are shown in Figure 3.12 and Table 3.6. The upper bound of the 95% confidence interval used the 97.5% value for slope and the 97.5% value for intercept, while the lower bound of the 95% confidence interval used the 2.5% value for slope and the 2.5% value for intercept. Of note is the mass gain that is estimated in the highest elevation band for the lower bound 95% confidence interval. The DD model was also run for the period of 1912-1922 using the assumption that the glacier was 301 m higher in elevation based upon cumulative mass loss from the original 1912-2012 DD model. Temperature and snowpack were modelled to represent this increase in elevation change and the model results are shown in Table 3.5.

Table 3.6 Estimated mass loss for the period 1912-1922 using a range of DD models. (Mass loss in m w.e.).

Model	Elevation less than 2573 m	Elevation greater than 2754 m	Mean Mass Loss
Upper Bound 95% Confidence interval	65.4	55.4	61.6
Lower Bound 95% Confidence interval	16.9	-0.1	10.7
Temperature estimate used in DD Model	39.9	21.0	33.2
1912 Glacier Elevation	27.6	11.6	21.9

An ETI model was also run using the 1912 estimated glacier geometry with associated temperature and snowpack, and albedo calculated for a higher elevation (+301m) glacier. The temperature and snowpack were estimated using the same techniques as described in Chapter 2, see also Figure 2.10, while the albedo was assumed to be 0.6, old clean wet snow, for the beginning of the melt season and 0.35, clean ice, after the snowpack had melted. This differs from the original ETI model in that a value of 0.35 was used only for the elevation above 2550m while elevations below 2550 m used a value of 0.20, debris covered ice. See Figure 3.13 for the results.

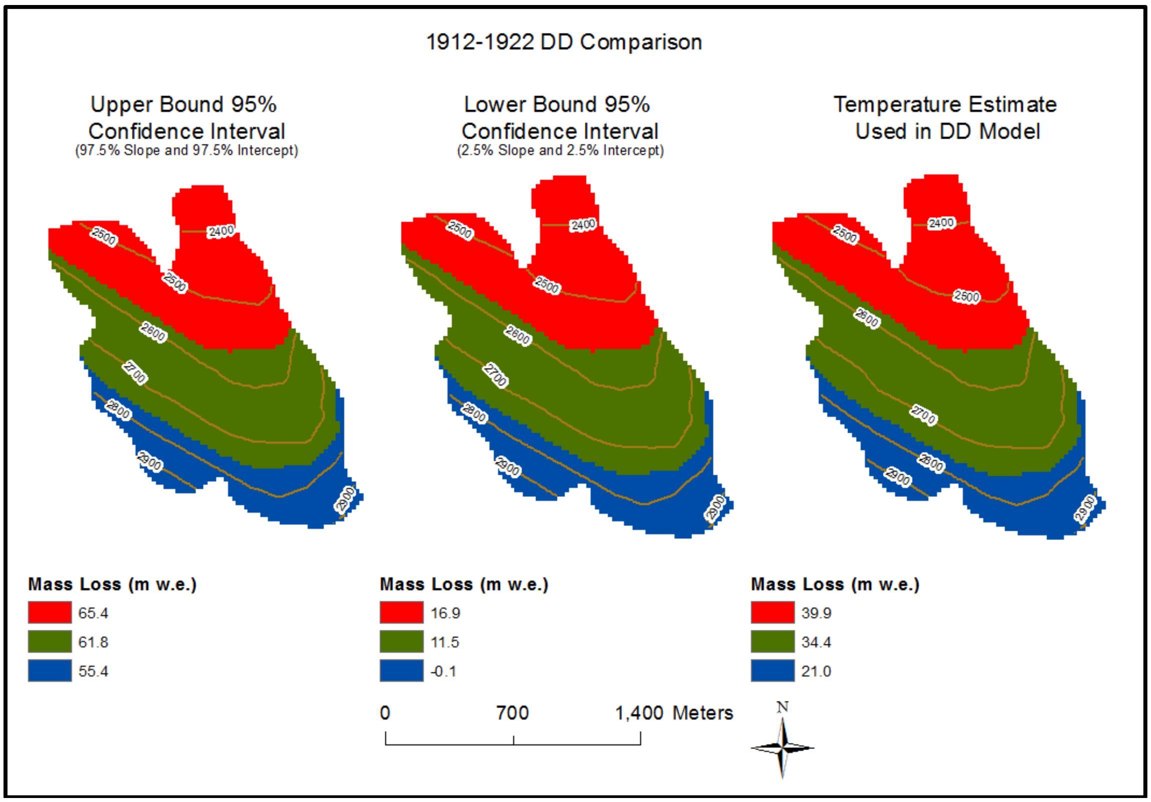

Figure 3.12 Estimated mass loss for the period 1912-1922 for Robertson Glacier with three different sets of temperature data. Left panel is with a high temperature estimate, 97.5% slope and 97.5% intercept value from linear regression. Middle panel is with a low temperature estimate, 2.5% slope and 2.5% intercept value from linear regression. Right panel is using the original temperature estimate.

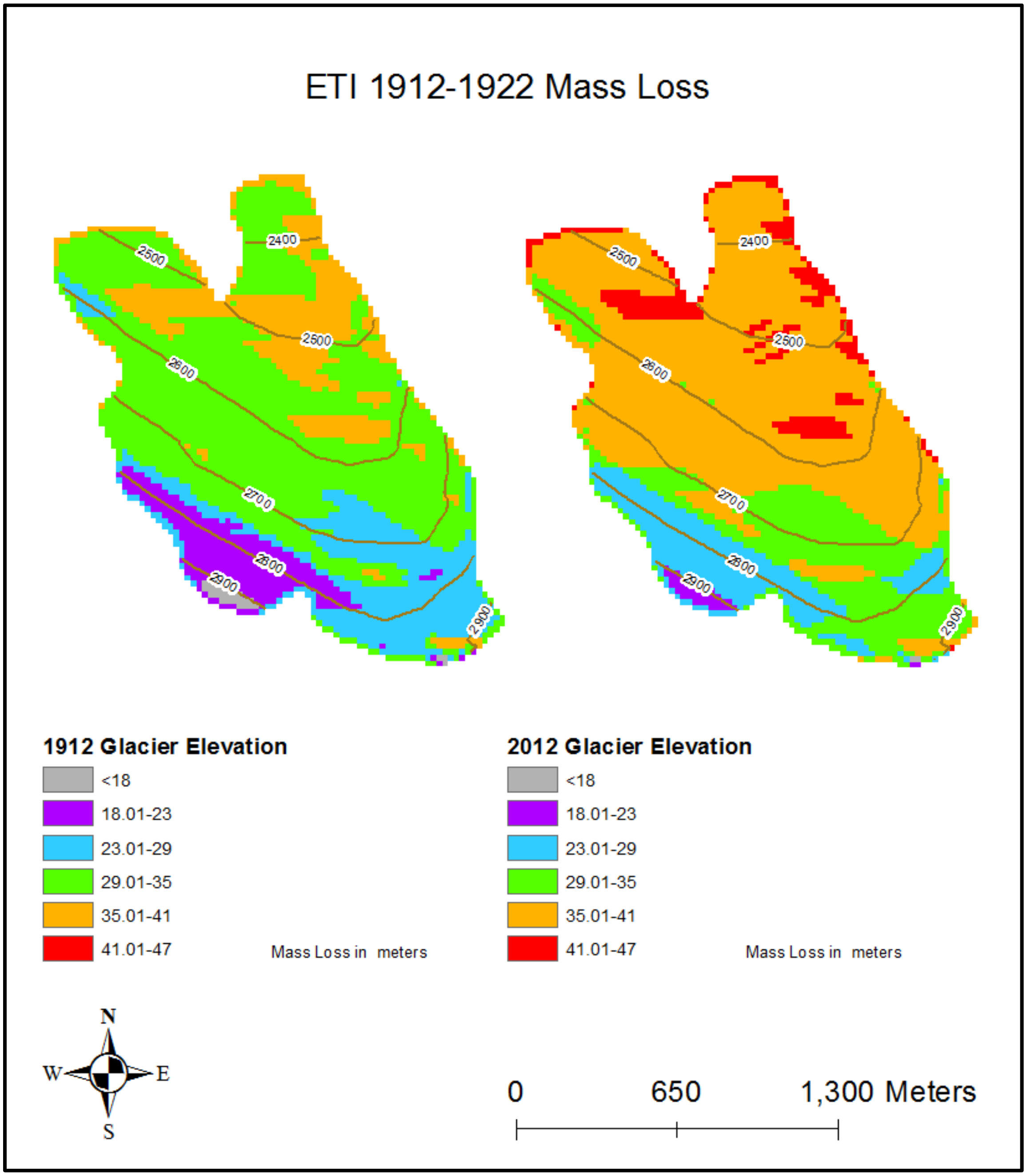

Figure 3.13 Comparison of ETI modeled mass loss for Robertson Glacier for the period 1912-1922 using a modified glacier elevation for 1912 (left panel) and using the 2012 glacier elevation (right panel).

The efficiency criterion R^2 from Nash & Sutcliffe (1970) was used to assess the performance of different values for the SRF and TF parameters, and is defined as:

$$\boldsymbol{R^2 = 1 - \frac{\sum_{i=1}^{n}(M_{ri} - M_{si})^2}{\sum_{i=1}^{n}(M_{ri} - \bar{M}_{ri})^2}} \tag{6}$$

where M is melt rate and subscripts r and s refer to the measured melt and modeled melt rate respectively. The bar refers to the mean, and n is the number of time-steps for which R^2 is calculated, in this instance n=10. This criterion has been used previously in glaciological studies by Hock (1999) and Pellicciotti et al. (2005) to assess the model performance, R^2 is the percentage of the response variable, modeled melt, that is explained by a linear model. By selecting the values of SRF and TF with the highest associated R^2, the values are optimized and predict the lowest percentage of variation between the measured and modeled values.

A range of values (0.001 – 1.0 m^2 mm (Wh^{-1}) day^{-1}) was tested for SRF while holding all other values and parameters in the ETI model constant to evaluate the sensitivity of SRF (Figure 3.15). This wide range of values was chosen to determine the optimal value of SRF. R^2 is above 0.8 for SRF values 0.008 - 0.011 m^2 mm Wh^{-1} day^{-1}, showing limited sensitivity in this range, but the R^2 declines rapidly above and below this range indicating greater sensitivity in SRF (Figure 3.14).

A range of values (0.5 – 8.5 mm w.e. day^{-1} $°C^{-1}$) was tested for TF while keeping SRF and α constant in the ETI model and the efficiency criterion R^2 was determined, (Figure 3.15). This wide range of values was chosen to determine the optimal value of TF. TF is relatively insensitive in the range between 1.5 and 2.5 mm w.e. day^{-1} $°C^{-1}$ with R^2 only varying between 0.8 and 0.87, however TF values outside of this range show low efficiency; R^2 is reduced to 0.26 when TF is 0.5 and down to 0.22 when TF is at 3.5. These results contrast with the findings of Pellicciotti et al. (2005), where they determined that TF had a high efficiency value, ($R^2 = 0.9$) for the range 0.01-0.09 mm h^{-1} $°C^{-1}$ which, corresponds to a range of 0.24 – 2.16 w.e. day^{-1} $°C^{-1}$, indicating their model was relatively insensitive over a wider range of values than in the model for Robertson Glacier.

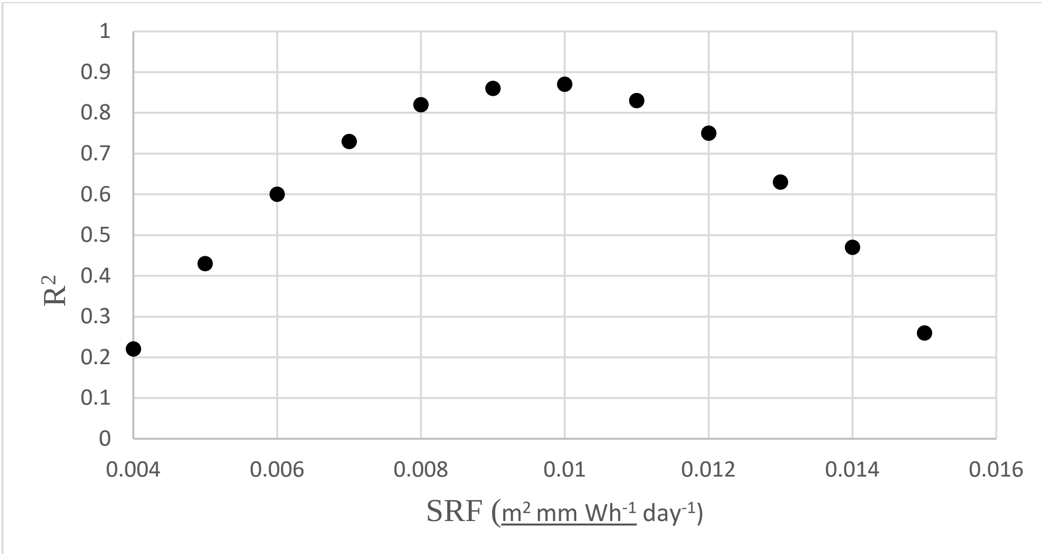

Figure 3.14. Efficiency criterion R^2 from Nash & Sutcliffe (1970) for SRF values in the ETI model, where TF and α were held constant. SRF values with a corresponding $R^2 > 0.8$ were considered optimal.

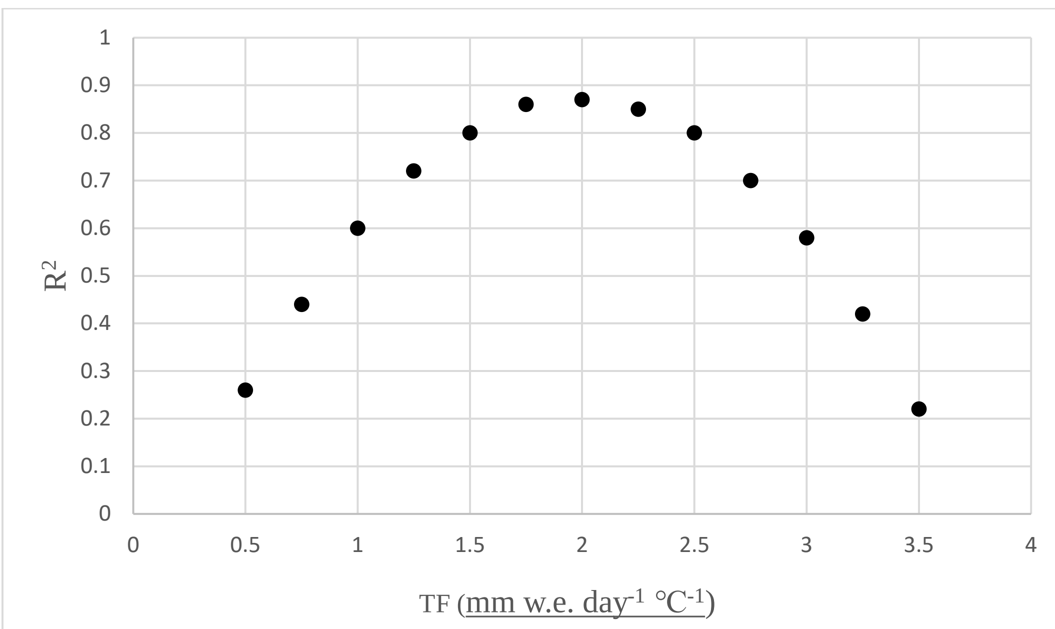

Figure 3.15. Efficiency criterion R^2 from Nash & Sutcliffe (1970) for TF values in the ETI model, where SRF and α were held constant. TF values with a corresponding $R^2 > 0.8$ were considered optimal.

CHAPTER 4 – DISCUSSION

The thesis aimed to determine if an ETI model with *a priori* knowledge could effectively model historic glacier melt with only a regional temperature data set as a measured input (Table 4.1). Temperature index models over simplify the complex physical process that are involved in surface melt, but require only limited inputs, mainly temperature. The ETI utilizes temperature but also incorporates incoming shortwave radiation and outgoing shortwave radiation based upon surface albedo. The goal of the thesis was to evaluate the differences in modeled melt, when parameterizing shortwave radiation and albedo without direct measurements relative to the DD model. Table 4.1 illustrates the different combination of inputs used in the ETI and the DD model for two different time periods, 1912-2006 and 2007-2012. Shortwave radiation was measured at the Robertson AWS and modeled for Robertson Glacier during the period 2007-2012 and for the period 1912-2006 shortwave radiation was parameterized using the daily mean shortwave radiation for each day in the period 2007-2012. Albedo was parameterized using *a priori* knowledge of the ice cover conditions (e.g. see Figure 2.8) and values from literature. Temperature was measured at the Banff AWS and modeled for Robertson Glacier using linear regression. Snowpack data was modeled using ClimateAB which relies on PRISM.

Table 4.1 Different types of inputs used for the four models used in this analysis.

Input	ETI (2007-2012)	DD (2007-2012)	ETI (1912-2006)	DD (1912-2006)
Shortwave Radiation	Modeled	NA	Parameterized	NA
Albedo	Parameterized	NA	Parameterized	NA
Temperature	Measured at regional scale and synthesized	Measured at regional scale and synthesized	Measured at regional scale and synthesized	Measured at regional scale and synthesized
Snowpack	Modeled with PRISM	Modeled with PRISM	Modeled with PRISM	Modeled with PRISM

The DD model is widely accepted and has been used in numerous studies to model melt (Braithwaite, 1981; Braithwaite, 1995; Johannesson et al. 1995; Hock, 1999), while the ETI is newer but has also been used with measured inputs to model melt (Pellicciotti et al. 2005). The ETI model was run for 100 years for Robertson Glacier with temperature being the only measured input for 94 years (Table 4.1). This period was chosen because it was the longest instrumental temperature record available within proximity to the glacier. This was compared to the DD model that only had direct measurements for three months during one melt season of the 100 years with the rest of the data determined by linear regression with the Banff AWS.

The ETI estimated greater mass loss than the DD model in all but 20 years, on average by 177 mm w.e. more per year. It is difficult to determine how well the ETI models actual melt as there were only ten data points collected of melt over the course of one month in summer 2012 to compare to the model. However, during this short period, the ETI modeled 87% of measured melt using the measured air temperature on the glacier and modeled solar radiation. These findings are at least consistent with the Pellicciotti et al., (2005) study at Haut Glacier d'Arolla, Switzerland, that used an ETI model to estimate melt over one summer melt season. Pellicciotti et al., (2005) found that when shortwave radiation and temperature were measured, the ETI modeled 90% of surface melt and this was reduced to 80% when shortwave radiation and temperature were parameterized. However, it is difficult to determine how representative the results of the month-long comparison at Robertson Glacier are over a century time period.

Advantages and Disadvantages of the ETI Model relative to the DD model

The ETI and DD models both require air temperature data that can be measured at the glacier or measured at a nearby location and estimated through linear regression or lapse rates to estimate glacier air temperatures. However, the ETI model required more inputs, albedo, TF and SRF to be parameterized, measured, or estimated than the DD model where only the DDF was parameterized. The modeled results from the ETI, DD, and a satellite image of Robertson Glacier are shown in Figure 4.1, and the ETI is better at modeling spatial variability of melt and reflects topographic shading. The ETI model was limited by the resolution of the Digital Elevation Model, which for Robertson Glacier was 30 m^2, whereas the DD model was limited to discrete elevation bands, determined by the density of ablation stakes on the glacier with air temperature records, yielding only three different output values for the DD model.

Limitations to the ETI model are that it requires some *in situ* field studies and *a priori* knowledge of the glacier where the mass balance is being modelled. To parameterize albedo requires knowledge of the glacier surface conditions, debris covered, clean, blue ice or snow covered during the melt season, however one can parameterize these based-on season/elevations. For the TF and SRF factors, one needs to know (i) shortwave radiation, which is difficult to parameterize without a nearby AWS that records incoming shortwave radiation and (ii) ablation rates which can be measured through a combination of methods, via automatic techniques at an AWS using an ultrasonic depth gauge, or snow pillow or manually on the ice via the straightedge method. In this study, there was a 6-year record of incoming shortwave radiation data from the Robertson AWS, 1 km down valley from the glacier and 10 measurements of ablation on the glacier, during summer 2012.

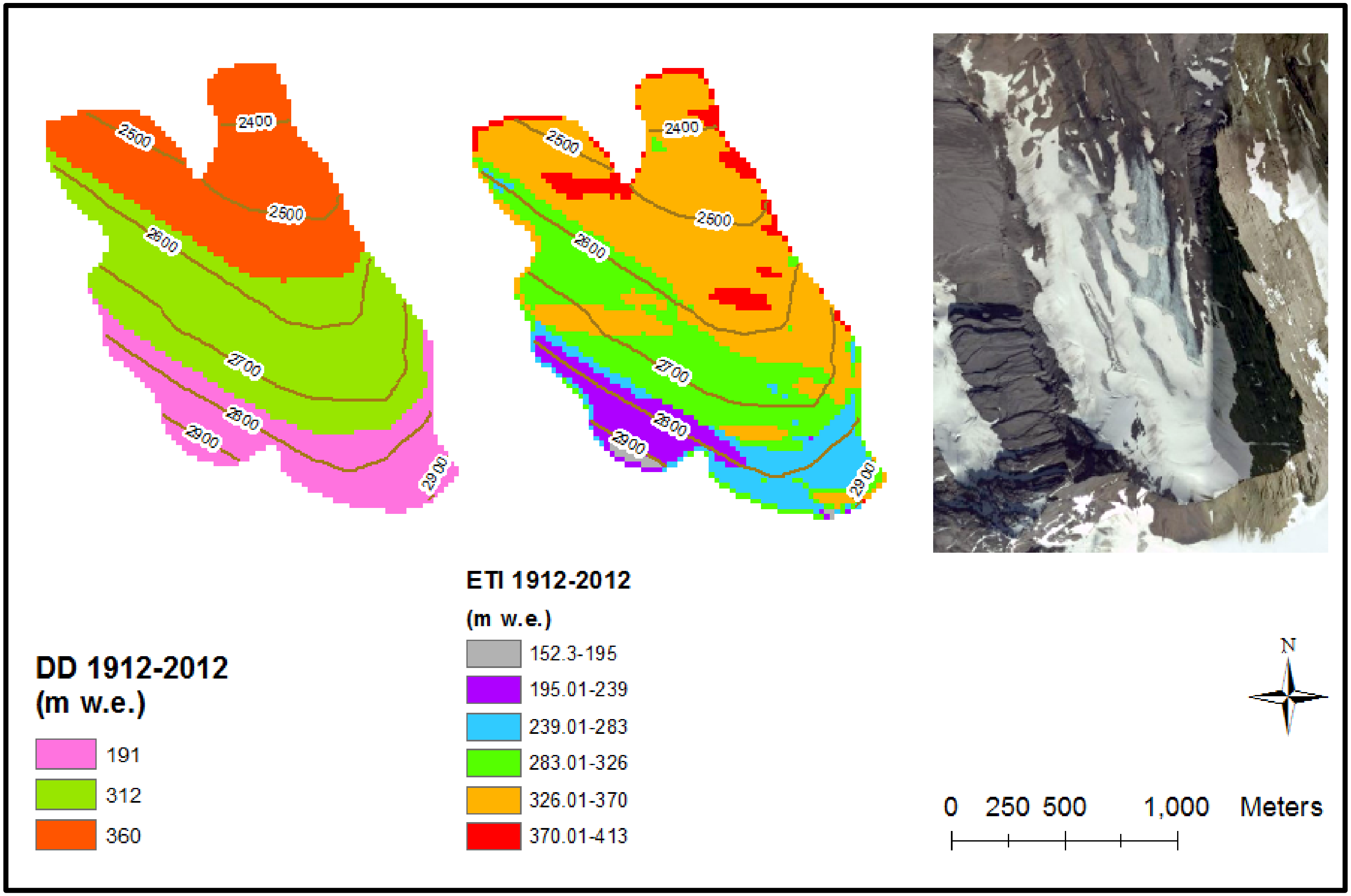

Figure 4.1 Modeled mass loss of Robertson Glacier. Left panel, DD model for period 1912-2012, Center panel, ETI model for period 1912-2012, Right panel, Satellite image of Robertson Glacier. (Google, 2016).

Comparison with Other Mass Balance Records in the Southern Canadian Rockies and Globally

Unfortunately, there are no long-term mass balance records of smaller stand-alone valley glaciers in the southern Canadian Rockies, however, there are two years of mass balance data published for the adjacent Haig Glacier for 2002 and 2003 (Shea et al., 2005). The mass loss measured for the Haig Glacier was 330mm w.e. in 2002 and 1530mm w.e. in 2003, and these values are significantly lower than the estimates for mass loss for Robertson Glacier for the same time period using the DD or ETI model. This suggests there are limitations to the DD and ETI model in terms of parameterization and/or potential errors in input data. Shea et al., (2005) measured both winter and summer balance to generate annual mass loss, and the measured winter balance i.e. snowpack thickness was significantly greater than the PRISM estimate for the same location, on average 220% greater for the two years (Table 3.4). The PRISM estimates of snowpack for 2002 and 2003 for both the Haig Glacier (2640m) and Robertson Glacier (2866m), which are only 2.5km apart, are similar, within 30 mm w.e. Although it is recognized that there is only two years of data it strongly suggests that the snowpack thickness estimates using PRISM for the DD and ETI models for Robertson Glacier are greatly underestimating the real snowpack depth, leading in part to the large estimates of mass loss.

Comparison of the modeled mass loss data for Robertson Glacier to the only longer term mass balance record in the region, Peyto Glacier also highlights a significant mismatch in mass loss (Figure 4.2)

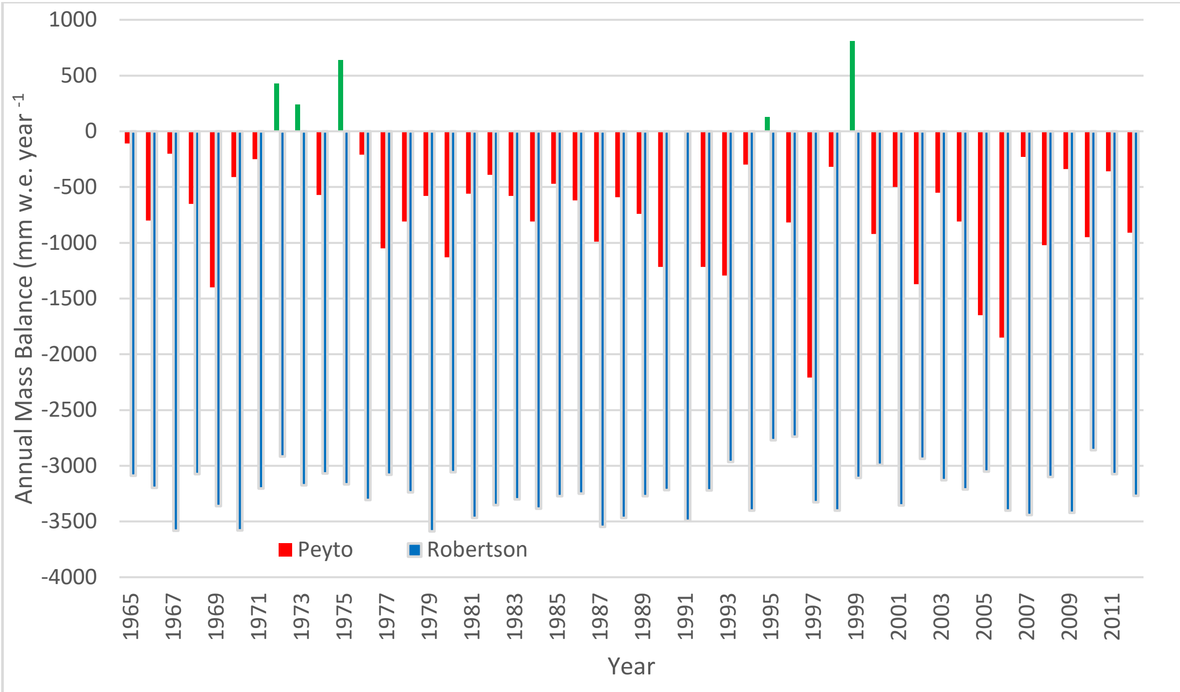

Figure 4.2. Annual Mass balance measured at Peyto Glacier and estimated for Robertson Glacier using a DD model 1966-2012. Peyto Glacier data courtesy World Glacier Monitoring Service, 2016. Positive mass balance years (1973, 1974, 1976, 1996, and 2000) for Peyto Glacier are shown in green.

Peyto Glacier, an outflow glacier from the Wapta Icefield 133 km northwest of Robertson Glacier has a record of mass balance from 1965-2015, Figure 4.2 (Young 1981; Demuth et al, 2006, World Glacier Monitoring Service, 2016). Peyto Glacier ranges in elevation from 2125 m to 3185 m faces northeast (aspect, 45°), (Young, 1981), compared to Robertson Glacier which ranges from 2366 m to 2900 m and an aspect of 340°. A direct comparison of mass balance between Robertson and Peyto Glacier has significant limitations, because Peyto Glacier is fed by an icefield and has a contributing area of 247 km^2 (Hopkinson & Demuth, 2006), however, given the paucity of mass balance records in the region it is the only one than one can make a comparison with. Peyto Glacier has had five positive mass balance years since 1965 (Figure 4.2), they were

1973, 1974, 1976, 1996, and 2000, with the greatest annual mass loss being approximately 2500 mm w.e., in 2015 (World Glacier Monitoring Service, 2016). This contrasts with the DD and ETI models for Robertson Glacier, where there were no years over the century of modelled outputs, in which the models predicted a positive balance, net mass added. During the period 2002-2012, Peyto Glacier lost 9.6 m w.e. (Figure 4.2), while the DD and ETI models for Robertson Glacier estimated losses of 32.6 m w.e. and 34.9 m w.e. respectively. The average annual mass loss at Peyto Glacier during this period was 0.88 m w.e., compared to model predictions of 2.9 m w.e. and 3.2 m w.e. mass loss for Robertson Glacier for the DD and ETI models respectively. Further, if one compares mass loss estimates for Robertson Glacier for the DD and ETI models ~ 3000mm w.e./year to the mean specific annual mass balance determined for 40 reference glaciers for the period 2001-2010, -740 mm w.e./year (WGMS, 2015) it is also clear that the modelled values for Robertson Glacier are high. Note, these reference glaciers are found in Canada, USA, Norway, Russia, European Alps, Sweden, China, Kazakhstan and Chile and all have received continuous long-term observations, 30 years or longer (WGMS, 2015).

To evaluate the effects of increased snowpack at Robertson Glacier on the mass loss estimates, the DD model was run for the period 2002-2012 under three scenarios. 1) using snowpack values of +220 % based on the Haig Glacier data (Table 3.4, Shea et al. 2005) 2) determining the snowpack thickness that would be required for the mean mass loss of Robertson Glacier to equal that of Peyto Glacier and 3) determining the snowpack thickness that would be required for the mean mass loss of Robertson Glacier to equal that of the WGMS mean mass loss of 740 mm w.e./year. In all cases the temperature and DDF values remained unchanged from the original model. The results can be seen in Tables 4.2, 4.3 and 4.4.

Table 4.2 DD Model run for Robertson Glacier 2002-2012 with snowpack estimates of +220%.

Year	**Mean Mass Loss**	**Mass Loss with Snowpack +220%**	**Difference**
2002	2938	1401	1537
2003	3129	1745	1384
2004	3212	1192	2020
2005	3051	981	2070
2006	3402	1399	2003
2007	3443	1239	2204
2008	3101	1201	1900
2009	3422	1168	2254
2010	2861	1254	1607
2011	3074	1254	1820
2012	3271	1254	2017
Mean	3173	1281	1892

Table 4.3. Comparison between modelled mass loss at Robertson Glacier and measured at Peyto Glacier for 2002-2012 and the snowpack thickness required to make mean mass loss equal.

Year	**Robertson Glacier Mean Mass Loss (mm w.e.)**	**Peyto Glacier Mean Mass Loss (mm w.e.)**	**% Difference Between Snowpack Required for Mean Mass Loss to Equal Peyto Mass Loss and PRISM Estimates**
2002	2938	1370	346%
2003	3129	550	425%
2004	3212	810	543%
2005	3051	1650	414%
2006	3402	1850	344%
2007	3443	230	671%
2008	3101	1020	481%
2009	3422	340	680%
2010	2861	950	435%
2011	3074	360	576%
2012	3271	910	514%
Mean	*3173*	*913*	*494%*

Table 4.4. Comparison of PRISM estimated snowpack thickness in the initial DD model with snowpack thickness required for Robertson Glacier mean mass loss to equal WGMS mean mass loss for 2002-2012.

Year	**Robertson Glacier Mean Mass Loss (mm w.e.)**	**Snowpack required for mean mass loss to equal 740 mm w.e. (mm w.e.)**	**% Difference between Snowpack required for mass balance to 740 mm w.e. and PRISM estimates**
2002	2938	2825	443%
2003	3129	3172	400%
2004	3212	3004	554%
2005	3051	2747	616%
2006	3402	3288	517%
2007	3443	3256	578%
2008	3101	2897	531%
2009	3422	3203	603%
2010	2861	2681	470%
2011	3074	2894	508%
2012	3271	3091	542%
Mean	*3173*	*3005*	*524%*

With 220% greater snowpack, the mean mass loss predicted for Robertson Glacier using the DD model is on average 1.892 m w.e per year from 2002-2012. In comparison, the DD model output indicated that the percent difference of snowpack for Robertson Glacier mean mass loss to equal the mean mass loss for Peyto Glacier and the WGMS reference glaciers was 494% and 524% respectively. The results of these modelling scenarios, indicate that there are likely additional factors other than snowpack thickness that could contribute to the high mass loss estimates for Robertson Glacier using the DD model.

The potential over estimation of mass loss at Robertson Glacier is likely due to a combination of factors, e.g., underestimation of snowpack thickness using PRISM, avalanche deposition, and elevation change of the glacier over the century. Some of these factors are compounding, in terms of the negative feedback they have on mass loss. For example, snowpack underestimation with PRISM and avalanche deposition of snow would greatly increase the snowpack at the beginning of the melt season and increase the albedo for a longer duration of the melt season, thus leading to decreased melt. With glacier surface elevation increases as one moves further back in time over the century, one could expect to see lower temperatures, higher snowfall, and higher albedo values all of which lead to decreases in mass loss. These are discussed further in the next section.

Limitations to the Application of DD and ETI Models at Robertson Glacier

Elevation Change

One of the greatest limitations of the models when attempting to estimate the previous 100-year period of mass balance is the lack of glacier surface elevation change over time. The DD model output predicted that Robertson Glacier had lost 360 m at the terminus and 191m in the upper part of the glacier near the col, Figure 3.6. If this mass loss and elevation decrease had actually occurred, then one would expect to see both lower air temperatures and greater snowfall increasing as one moved back in time. The combination of lower temperatures and higher snowfall, resulting from the higher initial elevation would reduce the amount of mass loss as was shown in Figure 3.12. Further at Robertson, the lower one-third of the glacier is currently highly debris-covered and thus has a low albedo, but with higher elevation, more snowfall and less melt, one would expect a greater area to be covered by snow and ice, thus increasing albedo and decreasing mass loss through melt (Figure 3.12). Another effect of increased glacier thickness and realistically its lateral extent, would be a reduction in reflected radiation from the dark rock walls that surround Robertson Glacier, also reducing melt and thus mass loss.

Albedo

Albedo was parameterized in the ETI model and only three possible values were used, 0.2, 0.35 and 0.6, these values could overestimate melt during the latter part of the melt season when new snowfall events are likely. For example, during the 2012 summer melt season there was a new snowfall event on September 11th, 2012 with the new snow remaining on the glacier through September 12th, halting melt on the glacier surface during that time. Although this is a singular example the cumulative effect of such events over a one-hundred-year record could be noteworthy. Jonsell et al., (2003) at Storglaciären, Sweden found that albedo over ice can have a day-to-day variability of greater than 20%. Pellicciotti et al. (2005) noted only a minor reduction of R^2 from 0.911 to 0.893 when changing from measured albedo to simply parameterizing albedo, however, this was for a point location on Haut Glacier d'Arolla, Switzerland over a time period of six weeks. However, in the Robertson study *a priori* knowledge of the glacier and values from the literature for albedo were chosen based on field observations, but no direct measurements of albedo, i.e. using upward and downward facing radiometers (Cuffey & Paterson, 2010) were made. Gardner & Sharp (2010) state that using these parameterizations are limited in their applicability because they are based on statistical fits to albedo measurements from specific locations and time periods. The highest albedo was 0.6 for old clean wet snow which would most likely be encountered at the beginning of the melt season. An albedo value of 0.2 was used for the debris covered terminus of the glacier which resulted in the high melt estimates seen (Figure 3.8). Figure 4.3 shows the sensitivity of albedo when all other values are held constant.

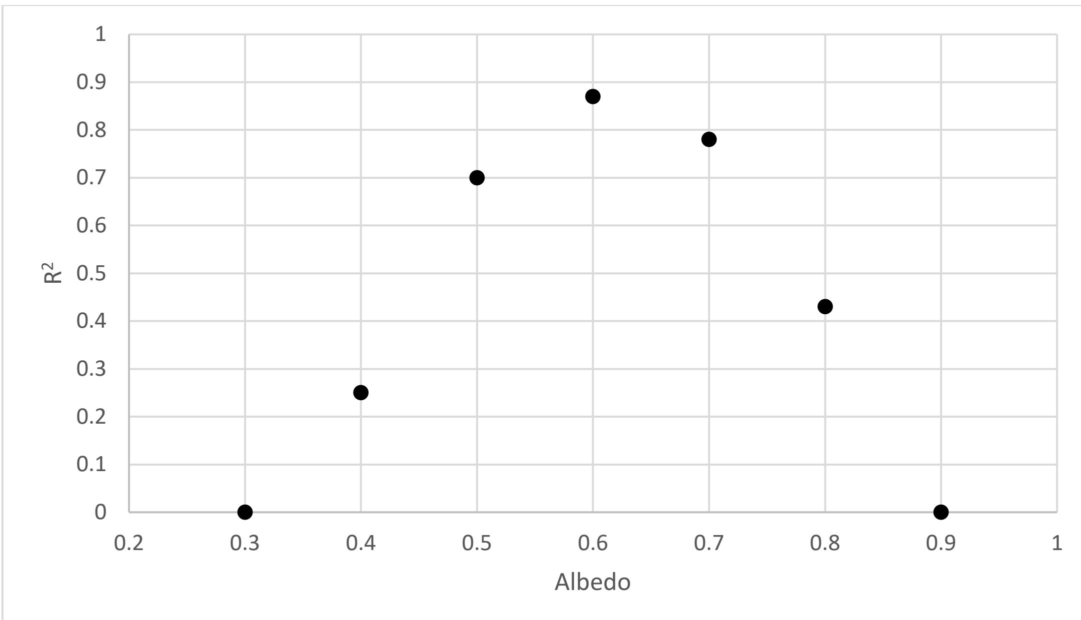

Figure 4.3. Efficiency criterion R^2 from Nash & Sutcliffe (1970) for albedo values in the ETI model, where TF and SRF were held constant. Albedo values with a corresponding $R^2 > 0.8$ were considered optimal.

A range of values (0.3 – 0.9) were tested for albedo in the ETI model, while keeping SRF and TF constant, and the efficiency criterion R^2 was determined, (Figure 4.3). R^2 is optimized at an albedo of 0.6, where the highest efficiency criterion R^2 was observed. At lower and higher values of albedo the efficiency criterion R^2 is significantly reduced, indicating model output is sensitive to this variable and thus its importance when trying to model mass loss. A new snow event as was described earlier would result in an albedo of 0.8 to 0.9 and would reduce the R^2 of the model to less than 0.5, indicating the model limitation. Heynen et al., (2013) found that the ETI model was most sensitive to albedo parameters when summer precipitation, rain and snow, is occurring and when cloud cover is significant and the temperature is near the threshold melting temperature of 0°C.

Avalanche Deposition

An additional variable that impacts the real mass balance at Robertson Glacier but that is not captured in the DD or ETI models is the effect of snow redistribution through avalanching. Avalanching causes rapid transport of glacier inputs (i.e. mainly snow) and their immediate conversion to much denser material, accelerating the conversion of snow to glacier ice (Hewitt, 2011). Avalanches are a relatively frequent phenomenon at Robertson Glacier, as observed on the west side of Robertson glacier numerous times during the 2012 melt season. The magnitude of this effect at Robertson remains unquantified, but in studies in other mountainous terrain, e.g. Hewitt (1994) in the Karakorum, as much as two thirds of ice was estimated to be derived from snow avalanches sourced from higher elevations. Given the lower vertical relief at Robertson Glacier relative to the Karakorum region one would not expect this effect to be as significant in terms of mass balance. However, avalanching has been shown to be important in other Alpine settings. For example, Purdie et al., (2015) found on Rolleston Glacier, New Zealand that the average snow depth in 2013 was 5.8 m with a standard deviation of 1.89 m, with snow depths near a headwall in excess of 12 m. These higher snow depths occurred directly below avalanche cones, demonstrating the role of avalanching in contributing to spatial snowpack variability and locally doubling the average value.

Debris Cover

Debris cover plays an important role in glacier melt rates because of the effect it has on albedo. In both the DD model and ETI model very high annual melt rates occur in the lower third of Robertson Glacier due to the debris covered surface conditions, an albedo value of 0.2 was used for the area of the glacier below 2550 meters to account for the surface conditions. While debris cover decreases albedo from 0.35 to 0.20 when compared to clean ice, it can become an insulator when it reaches a certain thickness. In a controlled experiment on Khumbu Glacier, Nepal Himalaya (5350 m) in May of 1999, ice ablation was measured under differing amounts of debris. Debris cover of 0-5 cm increases daily ice ablation while debris of greater than 10 cm greatly reduces ablation with 40 cm of debris cover representing only 33% of bare ice ablation (Kayastha et al. 2000). This insulating effect is likely occurring at Robertson Glacier already as much of the lowest reaches of the glacier are covered by debris of more than 10 cm (See Figure 2.8b).

Summary

A mass balance record for the past century at Robertson Glacier, Alberta, Canada was generated using a degree day (DD) model and an enhanced temperature-index (ETI) model. These two models were parameterized using measurements taken at Robertson Glacier, during the melt season of 2012. The DD model used temperature as the sole input, and an optimized degree day factor to model surface melt at Robertson Glacier. The temperature was measured during the melt season of 2012 and modeled for the previous 99 years using linear regression from an automatic weather station (AWS) from Banff, Alberta, Canada. The ETI model used the same temperature data from the DD model in addition to albedo, which was parameterized based upon *a priori* knowledge, incoming shortwave radiation and a shortwave radiation factor. Incoming shortwave radiation was measured at an AWS that was located one km down valley from the terminus of the glacier and has been in operation since 2007. Clear sky incoming solar radiation was modeled for the glacier using ArcGIS, this was then multiplied by a ratio of clear sky values divided by measured values at the Robertson AWS, thus giving an estimate of actual incoming shortwave radiation for each 30 m^2 grid cell on Robertson Glacier.

Both the DD and ETI models show significant mass loss over the study period, 1912-2012. The DD estimated a mean of 301 m w.e. of mass loss for Robertson Glacier while the ETI estimated a mean of 319 m w.e. mass loss. The ETI model estimated more mass loss than the DD model in all but 20 years of the 101-year study. The mass loss values are not greatly different between the models however the ETI model delivers greater spatial detail of mass loss than does the DD in places where topographic shading are important. Mass loss is likely overestimated using the DD and ETI models for the century time period due to a range of factors; elevation change of the glacier, underestimation of snowpack thickness (i) using PRISM data and (ii) due avalanche deposition of snow onto the glacier and albedo parameterization, and some of these factors are compounding in their effects.

Recommendations for Future Research

There is much opportunity for future research and modeling regarding the comparison of the DD model and ETI model at Robertson Glacier. The greatest improvement would be the deployment of multiple AWS on the glacier surface for multiple years. These stations could then measure albedo, incoming solar radiation, and temperature and would thus make the factor calculations (TF and SRF) much more robust. Another improvement would be the creation of a high-resolution DEM. 25-30 m^2 grid spacing resolution is robust when modelling a large area, such as Greenland, (Howat et al., 2014) however, when examining the relatively small Robertson Glacier, 3 km^2, a higher resolution DEM would be beneficial. The recent advances in drone mounted photography coupled with terrestrial photogrammetry can generate a DEM with a grid size of $1m^2$ (Chapuis et al 2010). In addition, determining snowpack thickness and how much of the snowpack at Robertson Glacier is derived from avalanches would be beneficial, and this could be done using visual observations of avalanche debris followed by ground penetrating radar for comparison with measured snowfall data at an AWS located on the glacier, i.e. Purdie et al. 2015. Ground penetrating radar would also determine the thickness of the glacier as well as bedrock topography, such as the work done by Marshall & White, (2010). This would be useful to compare with the estimated thickness derived from the volume-area scaling.

REFERENCES CITED

Alberta Environment. (2005). *Alberta Climate Model (ACM) to provide climate estimates (1961-1990) for any location in Alberta from geographic coordinates*. *Alberta Environment* (Vol. 53).

Arendt, A., & Sharp, M. (1999). Energy balance measurements on a Canadian high Arctic glacier and their implications for mass balance modelling. In *Interactions Between the Cryosphere, Climate and Greenhouse Gases IAHS Publication*, 165-172.

Attore, F., Alfo, M., De Sanctis, M., Francesconi, F., & Bruno, F. (2007). Comparison of interpolation methods for mapping climatic and bioclimatic variables at regional scale. *International Journal of Climatology*, *27*, 1825–1843.

Benn, D., & Evans, D. (2010). *Glaciers and Glaciation*. Routledge.

Bolch, T., Menounos, B., & Wheate, R. (2010). Landsat-based inventory of glaciers in western Canada, 1985-2005. *Remote Sensing of Environment*, *114*(1), 127–137.

Bow River. (2016). In *Encyclopedia Britannica Online*.

Braithwaite, R. J. (1981). On Glacier Energy Balance, Ablation, and Air Temperature. *Journal of Glaciology*, *27*(97), 381–391.

Braithwaite, R. J. (1995). Positive degree-day factors for ablation on the Greenland Ice-sheet studied by energy balance modeling. *Journal of Glaciology*, *41*(137), 153–160.

Braithwaite, R. J., Konzelmann, T., Marty, C., & Olesen, O. B. (1998). Errors in daily ablation measurements in northern Greenland, 1993-94, and their implications for glacier climate studies. *Journal of Glaciology*, *44*(148), 583–588.

Braithwaite, R. J., & Olesen, O. B. (1989). Calculation of Glacier Ablation from Air Temperature, West Greenland. *Glacier Fluctuations and Climatic Change*, 219–233.

Braithwaite, R. J., & Olesen, O. B. (1990). A simple energy-balance model to calculate ice ablation at the margin of the Greenland ice sheet. *Journal of Glaciology*, *36*(123), 222–228.

Braithwaite, R. J., & Zhang, Y. (2000). Sensitivity of mass balance of five Swiss glaciers to temperature changes assessed by tuning a degree-day model. *Journal of Glaciology*, *46*(152), 7–14.

Chapuis, A., Rolstad, C., & Norland, R. (2010). Interpretation of amplitude data from a ground-based radar in combination with terrestrial photogrammetry and visual observations for calving monitoring of Kronebreen, Svalbard. *Annals of Glaciology*, *51*(55), 34–40.

Chen, J., & Ohmura, A. (1990). Estimation of Alpine glacier water resources and their change since the 1870s. *Hydrology in Mountainous Regions*, *V*(193), 127–136.

Citterio, M., Paul, F., Ahlstrøm, A., Jepsen, H., & Weidick, A. (2009). Remote sensing of glacier change in West Greenland: Accounting for the occurrence of surge-type glaciers. *Annals of Glaciology*, *50*(53), 70–80.

Cuffey, K. M., & Paterson, W. S. B. (2010). *The Physics of Glaciers (Fourth Edition)* (Fourth, Vol. 1). Elsevier Science.

Daly, C., Gibson, W. P., Taylor, G. H., Johnson, G. L., & Pasteris, P. (2002). A knowledge-based approach to the statistical mapping of climate. *Climate Research*, *22*(2), 99–113.

Demuth, M. N., Keller, R., Munro, S., & Young, G. J. (2006). An assessment of the mass balance of Peyto Glacier (1966-1995) and its relation to recent and past-century climatic variability. In *Peyto Glacier: One Century of Science* (pp. 83–132). National Hydrology Research Institute.

Demuth, M., & Pietroniro, A. (1999). Inferring Glacier Mass Balance Using Radarsat: Results from Peyto Glacier, Canada. *Geografiska Annaler, Series A: Physical Geography*, *81*(4), 521–540.

Eriksson, M., Jianchu, X., Shrestha, A. B., Vaidya, R. A., Nepal, S., & Sandström, K. (2009). *The changing Himalayas: impact of climate change on water resources and livelihoods in the greater Himalayas*. International centre for integrated mountain development (ICIMOD).

Finsterwalder, S., & Schunk, H. (1887). Der Suldenferner. *Zeitschrift Des Deutschen Und Oesterreichischen Alpenvereins*, *18*, 72–89.

Fountain, A. G., & Tangborn, W. V. (1985). The Effect of Glaciers on Streamflow Variations. *Water Resources Research*, *21*(4), 579–586.

Fountain, A. G., & Vecchia, A. (1999). How many stakes are required to measure the mass balance of a glacier. *Geografiska Annaler*, *81*(4), 563–568.

Gardner, A. S., Moholdt, G., Cogley, J. G., Wouters, B., Arendt, A., Wahr, J., Berthier, E., Hock, R., Pfeffer, W., Kaser, G., Ligtenberg, S., Bolch, T., Sharp, M., Hagen, J., van den Broeke, M., & Paul, F. (2013). A Reconciled Estimate of Glacier Contributions to Sea Level Rise: 2003 to 2009. *Science*, *340*(6134), 852–857.

Gardner, A. S., & Sharp, M. J. (2010). A review of snow and ice albedo and the development of a new physically based broadband albedo parameterization. *Journal of Geophysical Research: Earth Surface*, *115*(1), 1–15.

Google. (2016). Google Earth.

Greuell, W., & Smeets, P. (2001). Variations with elevation in the surface energy balance on the Pasterze (Austria). *Journal of Geophysical Research*, *106*(D23), 31717.

Gutmann, E.D., Rasmussen, R.M., Liu, C., Ikeda, K., Gochis, D.J., Clark, M.P., Dudhia, J. and Thompson, G. (2012). A comparison of statistical and dynamical downscaling of winter precipitation over complex terrain. *Journal of Climate*, *25*(1), pp.262-281.

Hendriks, J. P. M., & Pellikka, P. (2007). Semi-automatic glacier delineation from Landsat imagery over Hintereisferner in the Austrian Alps. *Zeitschrift Fur Gletscherkunde Und Glazialgeologie*, *41*, 55–75.

Hewitt, K. (1994). Altitudinal organization of Karakoram geomorphic processes and depositional environments. In *Shroder JF Jr, ed. Himalaya to the Sea: Geology, Geomorphology and the Quaternary* (pp. 159–183). New York: Routledge.

Hewitt, K. (2011). Glacier change, concentration, and elevation effects in the Karakoram Himalaya, Upper Indus Basin. *Mountain Research and Development*, 31(3), 188-200.

Heynen, M., Pellicciotti, F., & Carenzo, M. (2013). Parameter sensitivity of a distributed enhanced temperature-index melt model. *Annals of Glaciology*, *54*(63), 311–321.

Hock, R. (1999). A distributed temperature-index ice-and snowmelt model including potential direct solar radiation. *Journal of Glaciology*, *45*(149), 101–111.

Hock, R. (2003). Temperature index melt modelling in mountain areas. *Journal of Hydrology*, *282*(1–4), 104–115.

Hock, R., & Holmgren, B. (2005). A distributed surface energy-balance model for complex topography and its application to Storglaciären, Sweden. *Journal of Glaciology*, *51*(172), 25–36.

Hock, R., Oerlemans, J., & Radic, V. (2008). Analysis of scaling methods in deriving future volume evolutions of valley glaciers, *54*(187), 601–612.

Hopkinson, C., & Demuth, M. N. (2006). Using airborne lidar to assess the influence of glacier downwasting on water resources in the Canadian Rocky Mountains. *Canadian Journal of Remote Sensing*, *32*(2), 212–222.

Hopkinson, C., & Young, G. J. (1998). The effect of glacier wastage on the flow of the Bow River at Banff, Alberta, *Hydrological Processes*, *12*, 1745–1762.

Howat, I. M., Negrete, A., & Smith, B. E. (2014). The Greenland Ice Mapping Project (GIMP) land classification and surface elevation data sets. *The Cryosphere*, *8*(4), 1509-1518

Hutchinson, M. F. (1995). Interpolating mean rainfall using thin plate smoothing splines. *International Journal of Geographical Information Systems*, *9*(4), 385–403.

Jeton, A. E., Watkins, S. A., & Huntington, J. (2006). *Evaluation of Precipitation Estimates from PRISM for the 1961-90 and 1971-2000 Data Sets, Nevada*. US Geological Survey. Scientific Investigations Report 2005-5291

Johannesson, T., Sigurdsson, O., Laumann, T., & Kennett, M. (1995). Degree-day glacier mass-balance modelling with applications to glaciers in Iceland, Norway and Greenland. *Journal of Glaciology*, *41*(138), 345–358.

Jonsell, U., Hock, R., & Holmgren, B. (2003). Spatial and temporal variations in albedo on Storglaciaren, Sweden. *Journal of Glaciology*, *49*(164), 59–68.

Kaser, G., Fountain, A., & Jansson, P. (2003). A manual for monitoring the mass balance of mountain glaciers by. *IHPVI Technical Documents in Hydrology*, (59), 135.

Kayastha, R. B., Takeuchi, Y., Nakawo, M., & Ageta, Y. (2000). Practical prediction of ice melting beneath various thickness of debris cover on Khumbu Glacier, Nepal, using a positive degree-day factor. *IAHS Publication*, *volume number?* 71-82.

Lang, H. (1986). Forecasting Meltwater Runoff from Snow-Covered Areas and from Glacier Basins. *River Flow Modelling and Forecasting*, 99–127, Springer Netherlands.

Laumann, T., & Reeh, N. (1993). Sensitivity to climate change of the mass balance of glaciers in southern Norway. *Journal of Glaciology*, *39*, 656–665.

Meier, M. F. Dyurgerov, M. B. Rick, U.K., O'Neel, S. & Pfeffer, W.T., Anderson, R. S. Anderson, S.P., and Glazoysky, A.F. (2007). Glaciers Dominate Eustatic Sea-Level Rise in the 21st Century. *Science*, *317*, 1064–1067.

Marshall, S. J. (2005). Recent advances in understanding ice sheet dynamics. *Earth and Planetary Science Letters*, *240*(2), 191–204.

Marshall, S. J., Sharp, M. J., Burgess, D. O., & Anslow, F. S. (2007). Near-surface-temperature lapse rates on the Prince of Wales Icefield, Ellesmere Island, Canada: implications for regional downscaling of temperature. *International Journal of Climatology*, *27*, 385–398.

Marshall, S. J., White, E. C., Demuth, M. N., Bolch, T., Wheate, R., Menounos, B., Beedle, M., & Shea, J. M. (2011). Glacier Water Resources on the Eastern Slopes of the Canadian Rocky Mountains. *Canadian Water Resources Journal*, *36*, 109–134.

Marshall, S., & White, E. (2010). Alberta Glacier Inventory and Ice Volume Estimation, Alberta Innovates, Energy and Environment Solutions.

Mbogga, M. S., Hansen, C., Wang, T., & Hamann, A. (2010). A comprehensive set of interpolated climate data for Alberta. *University of Alberta, Department of Renewable Resources. Edmonton, AB.*

Nash, J. E., & Sutcliffe, J. V. (1970). River Flow Forecasting Through Conceptual Models Part I-a Discussion of Principles. *Journal of Hydrology*, *10*, 282–290.

Ohmura, A. (2001). Physical Basis for the Temperature-Based Melt-Index Method. *Journal of Applied Meteorology*, *40*, 753–761.

Oke, T. R. (2002). *Boundary Layer Climates*. Routledge.

Ommanney, C. S. L. (2001). *Glaciers of the Canadian Rockies. In Williams, R.S. and Ferrigno, J.G. (eds.) Satellite Image Atlas of Glaciers of the World*. *Encyclopedia of the world's endangered languages*. U S Geological Survey Professional Paper 1386 J1.

Onset. (2010). HOBO Pro v2 User's Manual.

Nr, S., & Orheim, O. (1970). Glaciological investigations of Store Supphellebre, West-Norway. Ostrem, G. (1964). Glacio-hydrological Investigations in Norway. *Journal of Hydrology*, *2*, 101–115.

Pellicciotti, F., Brock, B., Strasser, U., Burlando, P., Funk, M., & Corripio, J. (2005). An enhanced temperature-index glacier melt model including the shortwave radiation balance: Development and testing for Haut Glacier d'Arolla, Switzerland. *Journal of Glaciology*, *51*(175), 573–587.

Purdie, H., Rack, W., Anderson, B., Kerr, T., Chinn, T., Owens, I., & Linton, M. (2015). The impact of extreme summer melt on net accumulation of an avalanche fed glacier, as determined by ground-penetrating radar. *Geografiska Annaler: Series A, Physical Geography*, *97*(4), 779-791.

Schytt, V. (1964?). Scientific Results of the Swedish Glaciological Expedition to Nordaustlandet, Spitsbergen, 1957 and 1958. *Geografiska Annaler*, *46*(3), 242–281.

Shea, J. M., Anslow, F. S., & Marshall, S. J. (2005). Hydrometeorological relationships on Haig Glacier, Alberta, Canada. *Annals of Glaciology*, *40*, 52–60.

Srivastava, D., Kumar, A., Verma, A., & Swaroop, S. (2014). Analysis of Climate and Melt-runoff in Dunagiri Glacier of Garhwal Himalaya (India). *Water Resources Management*, *28*(10), 3035–3055.

Takeuchi, Y., Naruse, R., & Skvarca, P. (1996). Annual air-temperature measurement and ablation estimate at Moreno Glacier, Patagonia. *Bulletin of Glacier Research*, (14), 23–28.

Tangborn, W. V, Krimmel, R. M., & Meier, M. F. (1971). A comparison of glacier mass balance by glaciological, hydrological and mapping methods, South Cascade Glacier, Washington. *Snow and Ice-Symposium-Neiges et Glaces*, (104), 185–196.

Vincent, C., & Vallon, M. (1997). Meteorological controls on glacier mass balance: empirical relations suggested by measurements on Glacier de Sarennes, France. *Journal of Glaciology*, *43*(143), 131–137.

Willis, I. C., Arnold, N. S., & Brock, B. W. (2002). Effect of snowpack removal on energy balance, melt and runoff in a small supraglacial catchment. *Hydrological Processes*, *16*(14), 2721–2749.

WGMS 2015. Zemp, M., Gärtner-Roer, I., Nussbaumer, S. U., Hüsler, F., Machguth, H., Mölg, N., Paul, F., and Hoelzle, M. (eds.), *Global Glacier Change Bulletin No. 1 (2012–2013)*. ICSU(WDS)/IUGG(IACS)/ UNEP/UNESCO/WMO, World Glacier Monitoring Service, Zurich, Switzerland, 230 pp.

Yarnal, B. (1984). Relationships Between Synoptic Scale Atmospheric Circulation and Glacier Mass Balance in South-western Canada During the International Hydrological Decade, 1965-74. *Journal of Glaciology*, *30*(105), 188–198.

Young, G. J. (1981). The Mass Balance of Peyto Glacier, Alberta, Canada, 1965-1978. *Arctic and Alpine Research*, *13*(3), 307–318.

APPENDICES

APPENDIX A

R CODE FOR AWS AND BANFF LINEAR REGRESSION

```
# Read in the data from a text file
prob1 <- read.table("c:/R/AWS_Banff.txt", header=T)

# aovdata <- data.frame(y,trt)
attach(prob1)
names(prob1)


# Case I: Fit the SLR model to the original data
fit1 <- lm(AWS~Banff)
summary(fit1)
# Generate confidence interval
library(nlme)
2^(confint(fit1)[c(2,4)])
par(mfrow=c(2,2))
plot(AWS~Banff,main="SLR line: Original Data")
abline(fit1,col="red")

plot(fitted(fit1),residuals(fit1),main="Residual Plot: Original Data")
abline(h=0)
qqnorm(resid(fit1),main="Normal Probability Plot")
hist(resid(fit1),main="Histogram of Residuals")

anova(fit1)



#### Plot 95% Confidence bands for the SLR line. ####
# Enter the degrees of freedom for MSE
dfMSE=2301

# Pick a xmax and xmin value covering range of X values
# Then generate 10000 values between xmin and xmax
xmin <- -20
xmax <- 25
new <- data.frame (Banff= seq(xmin,xmax,length=10000))


# Generate a CI for each of these 1000 X values
est.cis <- predict(fit1, newdata=new, se.fit=TRUE, interval="confidence")
schef.mult = sqrt(2*qf(.95,2,dfMSE)) # Scheffe multiplier

# Calculate confidence band values using the Scheffe multiplier
band.low <- est.cis$fit[,1]
```

```
band.hi <- est.cis$fit[,1] + schef.mult*est.cis$se.fit
round(cbind(new$Banff,band.low, band.hi),3)

# Plot the confidence band
par(mfrow=c(1,1))
plot(Banff, AWS, type="n", main="Working-Hotelling Confidence Bands",
xlab="Banff", ylab="AWS",
        abline(fit1),lty=1, lwd=2, col=5) # plot the fitted line
        lines(new$Banff, band.low, lty=1, lwd=2, col=6)
        lines(new$Banff, band.hi, lty=1, lwd=2, col=3)


# Case II: Fit the SLR model to the log transformed X data
fit2 <-lm(AWS~log(Banff), na.rm=TRUE)
summary(fit2)

# Confidence intervals for the intercept and slope
library(nlme)
log(2)*confint(fit2,level=.95)

par(mfrow=c(2,2))
plot(AWS~log(Banff),main="SLR line: log(Banff)")
abline(fit2)
plot(fitted(fit2),residuals(fit2),main="Residual Plot: log(Banff)")
abline(h=0)
qqnorm(resid(fit2),main="Normal Probability Plot")
hist(resid(fit2),main="Histogram of Residuals")


# Case III: Fit the SLR model to the log transformed Y data
fit3 <-lm(log(AWS)~Banff)
summary(fit3)

# Generate estimate and CI for multiplicative change (interpretation 1)
library(nlme)
exp(coefficients(fit3)[c(2)])
exp(confint(fit3)[c(2,4)])

# Generate CI for multiplicative change (interpretation 2)
exp(confint(fit3)[c(2,4)]) - 1

par(mfrow=c(2,2))
plot(log(AWS)~Banff,main="SLR line: log(AWS)")
abline(fit3)
```

```
plot(fitted(fit3),residuals(fit3),main="Residual Plot: log(AWS)")
abline(h=0)
qqnorm(resid(fit3),main="Normal Probability Plot")
hist(resid(fit3),main="Histogram of Residuals")


# Case IV: Fit the SLR model to log transformations of both variables

logAWS = log(AWS)
logBanff = log(Banff)

# Fit the regression model
fit4 <- lm(logAWS ~ logBanff)
summary(fit4)

# Generate confidence interval
library(nlme)
2^(confint(fit4)[c(2,4)])

# Plot the data with the regression line
windows()
par(mfrow=c(2,2))
plot(logBanff,logAWS,main="SLR Line: log(X),log(Y) Data")
abline(fit4)

# Make residual plots
plot(fitted(fit4),resid(fit4),
main="Residuals vs Predicted Values")
abline(h=0)
qqnorm(resid(fit4),main="Normal Probability Plot")
hist(resid(fit4),main="Histogram of Residuals")
```

APPENDIX B

PYTHON CODE FOR DD

```
#!/usr/bin/python
# -*- coding: utf-8 -*-
#Author:Ryan Scanlon
#Contact: ryan.s.scanlon@gmail.com

import arcpy,os,sys,shutil,time,multiprocessing,re
from arcpy.sa import Con
from arcpy.sa import Raster
arcpy.env.overwriteOutput = True
arcpy.CheckOutExtension("spatial")
try:
from openpyxl import load_workbook
except:
raise Exception("install the openpyxl module in your python system")



#Use below and do not change anywhere else.Just change the paths and



INPUT_TEMP_EXCEL_PATH = r"D:\Sept112016\ModelPart2\Temprt - Copy.xlsx"
INPUT_DEM_RASTER_PATH = r"D:\Sept112016\ModelPart2\DEM\dem_clip_11"
OUTPUT_TEMP_RASTER_FOLDER = r"D:\Sept112016\ModelPart2\OutputRasters"
TEMP_FOLDER_PATH = r"D:\Sept112016\ModelPart2\mytemporaryfolder"
#TF
Second_Discrete_variable = 4.8





#Do not chage below


#Loading temperature data
Temp_Data = []
temp_wb = load_workbook(filename=INPUT_TEMP_EXCEL_PATH, read_only=True)
temp_ws = temp_wb[temp_wb.sheetnames[0]]
for row in temp_ws.rows:
d = []
if len(row)>3:
```

```
for cell in row:
if cell.value == None:
pass
elif cell.value == 0:
d.append(0.000000)
elif isinstance(cell.value, float):
d.append(round(cell.value,6))
else:
d.append(cell.value)
Temp_Data.append(d)

#process collected excel data
Temp_Data= Temp_Data[1:]
seen = set()
Temp_Data = [x for x in Temp_Data if x[0] not in seen and not seen.add(x[0])]#
removing duplicate date
#Folder content deleter
def folder_content_deleter(folder_path):
for the_file in os.listdir(folder_path):
file_path = os.path.join(folder_path, the_file)
try:
if os.path.isfile(file_path):
os.unlink(file_path)
elif os.path.isdir(file_path): shutil.rmtree(file_path)
except Exception as e:
pass

#folder deleter
def purge(dirpth, pattern):
for f in os.listdir(dirpth):
if re.search(pattern, f):
pth = os.path.join(dirpth, f)
shutil.rmtree(pth, ignore_errors=True)
#gdb content deleter
def gdb_content_deleter(wrkspc):
for r,d,fls in arcpy.da.Walk(wrkspc, datatype="FeatureClass"):
for f in fls:
try:
arcpy.Delete_management(os.path.join(r,f))
except:
pass

#copy and group by year
def grouperByYear(input_folder_path, output_folder_path):
```

```
for dirpath, dirnames, filenames in arcpy.da.Walk(input_folder_path, topdown=True,
datatype="RasterDataset", type="GRID"):
for filename in filenames:
out_folder_name = re.findall(r'(?<=\g)\d{4}', filename)[0]
out_folder_path = os.path.join(output_folder_path,out_folder_name)
if not os.path.exists(out_folder_path):
print ("Creating and populating folder for year %s ......"%out_folder_name)
os.mkdir(out_folder_path)
in_data = os.path.join(dirpath,filename)
ou_feature_name = 'g'+re.findall(r'(?<=\g\d{4})\d{4}$',filename)[0]
out_data = os.path.join(out_folder_path,ou_feature_name)
arcpy.Copy_management(in_data, out_data)

#Union all yeraly rasters

def summer(inp_flder):
rst_files = []
for dirpath, dirnames, filenames in arcpy.da.Walk(inp_flder, topdown=True,
datatype="RasterDataset", type="GRID"):
for filename in filenames:
rst_files.append(filename)
inp_rasters = [os.path.join(inp_flder,t) for t in rst_files]
summed_raster = arcpy.sa.CellStatistics(inp_rasters, "SUM", "DATA")
outraster_name = 'Summed_'+os.path.split(inp_flder)[1]
outraster_path = os.path.join(inp_flder,outraster_name)
summed_raster.save(outraster_path)


#processing Second part
def times_worker(times_range_list):
#set temporary places, grid format needs a gdb for placing intermediate data
#folder_content_deleter(TEMP_FOLDER_PATH)
scratch_db_name = "Scratch_"+str(times_range_list[0][0])
arcpy.CreateFileGDB_management(out_folder_path=TEMP_FOLDER_PATH,
out_name=scratch_db_name, out_version="CURRENT")
scr_db = os.path.join(TEMP_FOLDER_PATH,scratch_db_name+".gdb")
arcpy.env.scratchWorkspace = scr_db
#set output db
out_db_name = "RData_"+str(times_range_list[0][0])
#arcpy.CreateFileGDB_management(out_folder_path=OUTPUT_TEMP_RASTER_FOL
DER, out_name=out_db_name, out_version="CURRENT")
#out_db = os.path.join(OUTPUT_TEMP_RASTER_FOLDER,out_db_name+".gdb")
out_db = os.path.join(OUTPUT_TEMP_RASTER_FOLDER,out_db_name)
if not os.path.exists(out_db):os.mkdir(out_db)
```

```
arcpy.env.workspace = out_db
for tdata in times_range_list:
T1 = float('%.6f'%tdata[1])
T2 = float('%.6f'%tdata[2])
T3 = float('%.6f'%tdata[3])
out_path = os.path.join(out_db,'g'+str(tdata[0]))
outRast_name = "in_memory\\%s"%out_db_name
arcpy.MakeRasterLayer_management(INPUT_DEM_RASTER_PATH,outRast_name)
output_second =
Con(Raster(outRast_name)<2573,T1,Con(Raster(outRast_name)<=2754,T2,T3))
final_temp_raster = output_second*Second_Discrete_variable
#save
final_temp_raster.save(out_path)
#cleaning
gdb_content_deleter(scr_db)


def main(cu, worker, d_range):
pool = multiprocessing.Pool(cu)
pool.map(worker,d_range,1)
pool.close()
pool.join()
if __name__ == '__main__':
core_usage = 5 #multiprocessing.cpu_count()
chunk_size = 1000
needed_cpu = int(round((len(Temp_Data)/chunk_size),0)+1)
offsetter = list(divmod(needed_cpu, core_usage))
cpu_distribution = [core_usage]*offsetter[0]+[offsetter[1]]
cpu_distribution = [cp for cp in cpu_distribution if cp!=0]#just remove zero
temp_data_range = [Temp_Data[i:i+chunk_size] for i in
range(0,len(Temp_Data),chunk_size)]
#times_worker(temp_data_range[0])
print (r"Doing raster math. It may take 3-7 hours.\
Stop using your cpu fo this time!..........")
loopcnt = 0
for cpu in cpu_distribution:
temp_data_range_splitted = temp_data_range[loopcnt:loopcnt+cpu]
if len(temp_data_range_splitted)>0:
main(cpu, times_worker, temp_data_range_splitted)
loopcnt+=cpu
#Cleaning
if arcpy.Exists("in_memory"):
arcpy.Delete_management("in_memory")
folder_content_deleter(TEMP_FOLDER_PATH)
```

```
#group by year
print ("\nGrouping raster math output by year for you. It may take 1-2 hours !........\n")
grouperByYear(OUTPUT_TEMP_RASTER_FOLDER, OUTPUT_TEMP_RASTER_F
```

APPENDIX C

PYTHON CODE FOR ETI

```
#!/usr/bin/python
# -*- coding: utf-8 -*-
#Author:Ryan Scanlon
#Contact: ryan.s.scanlon@gmail.com

import arcpy,os,sys,shutil,re
from arcpy.sa import Con
from arcpy.sa import Raster
from arcpy.sa import Times
arcpy.env.overwriteOutput = True
arcpy.CheckOutExtension("spatial")
try:
from openpyxl import load_workbook
except:
raise Exception("install the openpyxl module in your python system")



#Use below and do not change anywhere else.

INPUT_TEMP_EXCEL_PATH = r"C:\Model\Temperature Model Data
Non_negative.xlsx"

INPUT_SNOW_EXCEL_PATH = r"C:\Model\Snowfall Model Data.xlsx"

INPUT_DEM_RASTER_PATH = r"C:\Model\DEM\dem_clip_11"
INPUT_SHORTWAVE_RASTER_FOLDER = r"C:\Model\1912"

#SRF
First_Discrete_variable = .015

#TF
Second_Discrete_variable = 1.05

Temp_Folder = r"C:\Model\mytempfolder"



#Do not chage below
use = 'S'#'S'
```

```
INPUT_TEMP_EXCEL_PATH = (arcpy.GetParameterAsText(0) if use == 'T' else
INPUT_TEMP_EXCEL_PATH
)
INPUT_SNOW_EXCEL_PATH = (arcpy.GetParameterAsText(1) if use == 'T' else
INPUT_SNOW_EXCEL_PATH
)
INPUT_DEM_RASTER_PATH = (arcpy.GetParameterAsText(2) if use == 'T' else
INPUT_DEM_RASTER_PATH
)
INPUT_SHORTWAVE_RASTER_FOLDER = (arcpy.GetParameterAsText(3) if use ==
'T' else
INPUT_SHORTWAVE_RASTER_FOLDER
)
First_Discrete_variable = (arcpy.GetParameterAsText(4) if use == 'T' else
First_Discrete_variable
)
Second_Discrete_variable = (arcpy.GetParameterAsText(5) if use == 'T' else
Second_Discrete_variable
)
Temp_Folder = (arcpy.GetParameterAsText(6) if use == 'T' else
Temp_Folder
)

#Initializing some data
First_Discrete_variable = float(First_Discrete_variable)
Second_Discrete_variable = float(Second_Discrete_variable)
regex_match_pattern_sol_rstr = re.compile(u'g\d{4}')
regex_match_pattern_sol_rstr_melt = re.compile(u'\d{4}')
year_melt_raster_prefix = 'MeltR_'

#-----------------------------------------------------------------------------
#Loading temperature data
Temp_Data = []
temp_wb = load_workbook(filename=INPUT_TEMP_EXCEL_PATH, read_only=True)
temp_ws = temp_wb[temp_wb.sheetnames[0]]
for row in temp_ws.rows:
d = []
if len(row)>3:
for cell in row:
if cell.value == None:
pass
elif cell.value == 0:
d.append(0.000000)
elif isinstance(cell.value, float):
```

```
d.append(round(cell.value,6))
else:
d.append(cell.value)
Temp_Data.append(d)

#process collected excel temperature data
Temp_Data= Temp_Data[1:]
seen = set()
Temp_Data = [x for x in Temp_Data if x[0] not in seen and not seen.add(x[0])]#
removing duplicate date

#-----------------------------------------------------------------------------
#Loading snow data
Snow_Data = []
snow_wb = load_workbook(filename=INPUT_SNOW_EXCEL_PATH,
read_only=True)
snow_ws = snow_wb[snow_wb.sheetnames[0]]
for row in snow_ws.rows:
rw = [cell.value for cell in row]
Snow_Data.append(rw)


#process collected excel snowfall data
Snow_Data = Snow_Data[1:]
seen = set()
Snow_Data = [x for x in Snow_Data if x[0] not in seen and not seen.add(x[0])]#
removing duplicate year

#list the solar raster in a folder
solr_rad_files=[]
for r,d,fls in arcpy.da.Walk(INPUT_SHORTWAVE_RASTER_FOLDER,
topdown=True, datatype="RasterDataset", type="GRID"):
for fl in fls:
if regex_match_pattern_sol_rstr.match(fl):
solr_rad_files.append(fl)
solr_rad_files = sorted(solr_rad_files)
#-----------------------------------------------------------------------------
#Defining useful functions that will be called later
#Folder content deleter
def folder_content_deleter(folder_path):
for the_file in os.listdir(folder_path):
file_path = os.path.join(folder_path, the_file)
try:
if os.path.isfile(file_path):
```

```
os.unlink(file_path)
elif os.path.isdir(file_path): shutil.rmtree(file_path)
except Exception as e:
pass
#folder deleter
def purge(dirpth, pattern):
for f in os.listdir(dirpth):
if re.search(pattern, f):
pth = os.path.join(dirpth, f)
shutil.rmtree(pth, ignore_errors=True)
#gdb content deleter
def gdb_content_deleter(wrkspc):
for r,d,fls in arcpy.da.Walk(wrkspc, datatype="FeatureClass"):
for f in fls:
try:
arcpy.Delete_management(os.path.join(r,f))
except:
pass
#set temporary places, grid format needs a gdb for placing intermediate data
folder_content_deleter(Temp_Folder)
arcpy.CreateFileGDB_management(out_folder_path=Temp_Folder,
out_name="ScratchData", out_version="CURRENT")
arcpy.env.scratchWorkspace = os.path.join(Temp_Folder,"ScratchData.gdb")


def get_processing_extent(raster_name1,raster_name2):
arcpy.env.extent = raster_name1
area1 = arcpy.env.extent.polygon.area
arcpy.env.extent = raster_name2
area2 = arcpy.env.extent.polygon.area
if area1>area2:
arcpy.env.extent = raster_name1
else:
arcpy.env.extent = raster_name2


#processing Second part
def get_temp_raster(timeframe, tempdata_list, dem_file_path,
temp_discrete_multiplier):#timeframe = u'19120515'
for tdata in tempdata_list:
if long(timeframe) == tdata[0]:
T1 = tdata[1]
T2 = tdata[2]
T3 = tdata[3]
```

```
temperature_raster =
Con(Raster(dem_file_path)<2573,T1,Con(Raster(dem_file_path)<=2754,T2,T3))
temperature_raster_times = Times(temperature_raster, temp_discrete_multiplier)
return temperature_raster_times

def get_snow_data(yr, snowdata_list):
for yer in snowdata_list:
if int(yr) == int(yer[0]):
_S1 = yer[1]
_S2 = yer[2]
return _S1,_S2

def multiplier_descrete_var_first(in_rast,snow_discrete_multiplier):
rst = Times(in_rast, snow_discrete_multiplier)
return rst

#Albedo
def alpha_minus_raster_generator(dem_raster_path, meltraster_or_constant, snow_year,
snowdata_list_data):
alpha1 = 0.60
alpha2 = 0.20
alpha3 = 0.35
S1 = get_snow_data(snow_year, snowdata_list_data)[0]
S2 = get_snow_data(snow_year, snowdata_list_data)[1]
output_dem_snow = Con(Raster(dem_raster_path)<2608,S1,S2)#chk
output_aplha =
Con(output_dem_snow>meltraster_or_constant,alpha1,Con(output_dem_snow<2550,alp
ha2,alpha3))
alpha_minus_rst = 1-output_aplha
return alpha_minus_rst

#copy and group by year
def getSumRasters(input_folder_path):
pattern = re.compile('meltr_\d+')
sumpathlist = []
finalmelt=0
for dirpath, dirnames, filenames in arcpy.da.Walk(input_folder_path, topdown=True,
datatype="RasterDataset", type="GRID"):
for filename in filenames:
if pattern.match(filename):
pth = os.path.join(dirpath,filename)
sumpathlist.append(pth)
for rst in sumpathlist:
finalmelt+=Raster(rst)
```

```
return finalmelt

if __name__ == '__main__':
iteration_counter = 0
melt = 0
yearname = ''
total_rast = len(solr_rad_files)
for solar_raster in solr_rad_files:
solar_raster_pth =
os.path.join(INPUT_SHORTWAVE_RASTER_FOLDER,solar_raster)
#Set raster processing extent
get_processing_extent(Raster(INPUT_DEM_RASTER_PATH),Raster(solar_raster_pth))

#setting and getting year and datestamp
context_year = os.path.split(os.path.split(solar_raster_pth)[0])[-1]
temperature_datestamp = context_year+solar_raster.replace('g','')
yearname = context_year
#processing starts
alpha_raster = alpha_minus_raster_generator(INPUT_DEM_RASTER_PATH, melt,
context_year, Snow_Data)
solar_radiation_raster = multiplier_descrete_var_first(solar_raster_pth,
First_Discrete_variable)
temperature_raster_second = get_temp_raster(temperature_datestamp, Temp_Data,
INPUT_DEM_RASTER_PATH,Second_Discrete_variable)
tempmelt = Times(solar_radiation_raster,alpha_raster)+temperature_raster_second
output_temp_melt_raster_path = os.path.join(Temp_Folder,
year_melt_raster_prefix+str(iteration_counter))
tempmelt.save(output_temp_melt_raster_path)
iteration_counter+=1
if use == 'T':
arcpy.AddMessage ('\nCompleted processing {0} ({1}) of total
{2}.....'.format(iteration_counter,solar_raster,total_rast))
else:
#pass
print '\nCompleted processing {0} ({1}) of total
{2}.....'.format(iteration_counter,solar_raster,total_rast)
finalmelt = getSumRasters(Temp_Folder)
output_melt_raster_path = os.path.join(INPUT_SHORTWAVE_RASTER_FOLDER,
year_melt_raster_prefix+yearname)
finalmelt.save(output_melt_raster_path)
purge(Temp_Folder, '.*')
folder_content_deleter(Temp_Folder)
if use == 'T':
arcpy.AddMessage(r"\nFinished Processing!")
```

```
else:
print "\nFinished Processing!"
```